EXPLORATORY STUDY OF DEEP BRAIN STIMULATION IN THE *SYNGAP1*$^{+/-}$ MOUSE MODEL OF AUTISM SPECTRUM DISORDER USING ELECTROPHYSIOLOGY

by

Umm E Hani Abdullah

A Thesis

Submitted to the Faculty of Purdue University

In Partial Fulfillment of the Requirements for the degree of

Master of Science in Biomedical Engineering

Weldon School of Biomedical Engineering

West Lafayette, Indiana

May 2023

THE PURDUE UNIVERSITY GRADUATE SCHOOL
STATEMENT OF COMMITTEE APPROVAL

Dr. Tamara Kinzer–Ursem, Chair

Weldon School of Biomedical Engineering

Dr. Karin Ejendal

Weldon School of Biomedical Engineering

Dr. Maria Dadarlat Makin

Weldon School of Biomedical Engineering

Approved by:

Dr. Tamara Kinzer–Ursem

To my grandparents who raised me – Mohammad and Shaista
My loving parents – Sadaf and Noman
My best friend and husband – Zain
My brother Haris for inspiring me daily
My siblings, aunts and cousins for their eternal love and camaraderie
My in-laws Zubair and Saira for loving me as their own

ACKNOWLEDGMENTS

It has been a delightful journey working on a project that I had envisioned since years. It started when my younger brother started developing severe symptoms of autism spectrum disorder which did not improve despite years of behavioral therapy, special schooling, and antipsychotics. It was early on during his appointments with medical practitioners and as a first-generation student in my family, I used to think if neurosurgical approaches could be the correct approach to treat such ailments. I was extremely fortunate to pursue neurological surgery as a career and observe some of the neuromodulation procedures.

It was at Purdue my abstract ideas got scientifically polished in Dr. Tamara Kinzer-Ursem's lab. Our project got build from the ground up as her lab introduced me to the concepts of neuroplasticity and autism spectrum disorder. Dr. Kinzer-Ursem is one of those rare breeds of researchers who truly identifies and keeps the student's interests at heart. In her lab, I could flourish and hone my skills and conduct a pilot project that had not been commonly pursued at various institutes owing to its interdisciplinary nature. She kept my best interests in mind and advocated for a collaboration with Dr. Maria Dadarlat Makin that allowed me to do mice craniotomies – experiments I absolutely enjoy performing. It has been an incredible journey learning about biomedical engineering from incredible female investigators.

Though the most indebted I feel to is Dr. Karin Ejendal. She taught me many skills from scratch that many undergraduate students catch up with earlier. I understood the significance of ethical research practices with her, and I owe her my entire success up till now. I was truly fortunate to be mentored by an extremely knowledgeable yet humble individual. Since I have joined, her door always remains slightly open so students can come in anytime and discuss their progress at will.

I am also extremely grateful to the students of both Dr. Tamara Kinzer-Ursem's and Dr. Maria Dadarlat's labs along with the biomedical engineering community at Purdue. Their patience and camaraderie enabled me to succeed. A special note of gratitude goes to Shulan Xiao, Hammad Khan, Andrew Sivaprakasam, and Dr. Melinda Lake for explaining me signal processing as it relates to local field potentials and providing me their valuable expertise in formulating a custom-

script. The undergraduate students on the projects Erin Tobin and Kevin Cragg were also extremely diligent in their work and I wish them all the success.

Lastly, I express my sincere gratitude to the International Neuromodulation Society; particularly Dr. Robert Levy and Dr. Marc Russo who accepted my grant as the inaugural award. I sincerely wish the scientific questions listed in my thesis attain further progress and gain traction with other neurologists, neurosurgeons, biomedical engineers, and neuroscientists. For long, treatment-resistant ASD has had no treatment and I hope our research can solve part of the puzzle.

TABLE OF CONTENTS

LIST OF TABLES

LIST OF FIGURES

ABSTRACT

Syngap1$^{+/-}$ haploinsufficiency is phenotypically characterized by autism spectrum disorder (ASD), intellectual disability (ID), and epilepsy. SynGAP (Synaptic Ras GTPase-activating protein) is a protein that regulates function in synapses. In addition, SynGAP protein is an integral component of the post-synaptic density and its role in signaling pathway converges with other autism risk genes and consequently autism risk proteins. A critical gap exists to understand how electrical stimulation as part of the Hebbian theory, can induce neuroplasticity. Previously, success in alleviating self-injurious behavior along with facilitating speech formation was demonstrated in adolescent patients undergoing deep brain stimulation (DBS) of the basolateral amygdala (BLA). Therefore, we sought to develop a chronic DBS model in *Syngap1*$^{+/-}$ haploinsufficient mice that can be used to assess the behavior and proteomic correlates due to DBS in BLA. We optimized the DBS surgery and anesthetic requirements to ensure survival of *Syngap1*$^{+/-}$ mice as they are more susceptible to isoflurane anesthesia. Additionally, we optimized the DBS stimulation parameters in accordance with behavior responses from *Syngap1*$^{+/-}$ mice by performing multiple trials of DBS stimulation. These methods include recording of local field potentials from *Syngap1*$^{+/-}$ mice. Our local field potentials were found to be in the frequency range of 7 – 30 Hz. Future directions include verifying the role of DBS in producing theta oscillations for the purposes of memory retrieval.

1. INTRODUCTION

1.1 Autism Spectrum Disorder

Autism Spectrum Disorder (ASD) is a heterogenous group of disorders characterized by impairments in social cognition and repetitive behaviors [1]. The spectrum of these patients varies from high-functioning to low-functioning [2].

ASD is characterized by two common symptoms present in all patients with varying intensity: impaired social behavior and stereotypical repetitive movements that emerge early in life [1]. Many of these patients exhibit additional syndromes in that they have gastrointestinal abnormalities, heart defects, epilepsy, craniofacial, and urogenital abnormalities [3, 4] (Figure 1.1). A subset of patients display severe autism where the patients cannot speak, show aggression, and injure themselves and others [5, 6]. In addition, an overwhelming 31% of patients with ASD present with intellectual disability (ID) and remain non-verbal – though some studies suggest the prevalence of co-occuring ASD and ID can be as much as 70% [7]. This results in an untreatable non-syndromic ID (NSID) caused by autosomal recessive and X-linked genes [8]. Moreover, self-injurious behavior (SIB) is a debilitating aspect prevalent in 35-50% of patients with ASD [9]. Therefore, a critical gap exists to assist and manage patients exhibiting the spectrum of this disease. Low functioning ASD patients rely on antipsychotics, anticonvulsants, and mood stabilizers, yet still present with refractory symptomatology causing a reduced quality of life and burden on caregivers [10].

The hallmark of ASD pathophysiology is characterized by a confluence of genetic and environmental aberrations resulting in in early brain development perturbations [11]. A few autosomal dominant genes have been characteristically implicated in autism. This includes fragile X syndrome and tuberous sclerosis where ASD remains a dominant phenotype [12]. Many of these genes converge at common molecular pathways in the post-synaptic density [13]. This is significant as it shows perturbing one pathway will result in changes downstream, affecting other common pathways [13].

As yet, there has been no cure established for ASD, rather interventions exist to best integrate these individuals into society and provide support for their symptoms. Pharmacological and behavioral interventions are the most commonly employed strategies for this disorder [14, 15].

Medications to treat ASD include antipsychotics such risperidone. However, since patients cumulatively take antipsychotics since years it results in side effects including metabolic resistance that can be detrimental to an already existing ASD syndrome. Therefore, doses must be given below a certain threshold per day [14]. Additionally, a unified framework of treating ASD has not yet developed [1, 2].

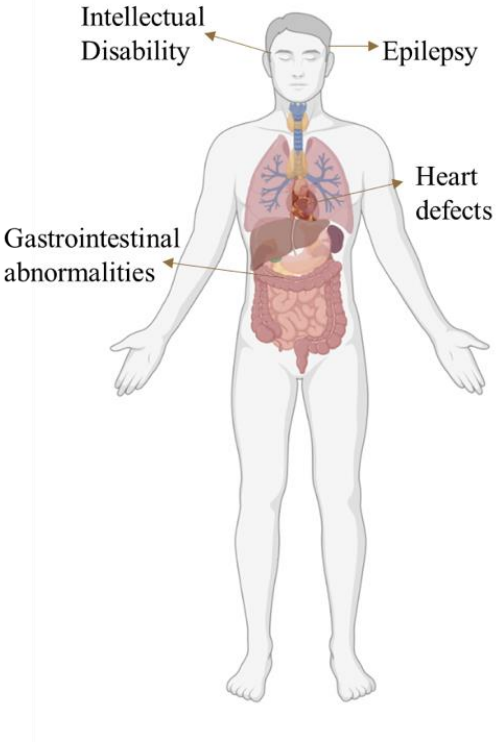

Figure 1.1: ASD is a syndromic disease that causes several related diseases with varying symptoms. These symptoms are not limited to the central nervous system. Other systems affected included the gastrointestinal and cardiovascular systems. Moreover, patients exhibit a spectrum of severity. Created and adapted in Biorender.com

1.2 Clinical Significance of Deep Brain Stimulation

Electrical stimulation of the brain has been used since the 19th century. Deep brain stimulation (DBS) is an invasive neurosurgical procedure, that involves implantation of unipolar electrodes to provide chronic stimulation [16]. It has traditionally been used for movement disorders. Here, it was noted that low frequency stimulation worsened the tremors as it can excite the nearby neurons, while high frequency improved the tremors by inducing a reversible lesion at the subthalamic nucleus [16, 17]. The history of DBS is characterized by a phase in the 20th century when psychosurgery, however, was discredited due to adverse outcomes related to paralysis.

Therefore, it was postulated that lesioning is not an effective way to treat such disorders. With the advent of pharmaceutics, Parkinson's disease got treated instead with pharmacological drugs instead of surgery [16, 17]. However, in the 1980s, resistance to levodopa started developing. Therefore, by 1990s, more traction started to gain towards DBS surgeries [16, 17].

Interestingly, while DBS immediately ameliorates tremors in Parkinsonian disease, recent literature has demonstrated off-targets of DBS cause personality changes [18]. As a result of these observed mood changes, DBS is now being further investigated for treatment-resistant psychiatric disorders such as depression and obsessive-compulsive disorder (OCD) [19].

The exact mechanisms by which DBS provides benefit to neurological disorders remain yet to be elucidated. Though, Hebbian theory suggests neurons achieve plasticity as 'neurons that fire together, wire together' giving rise to the idea that it is mimicking natural firing [20]. Additionally, DBS is postulated to induce neuroplasticity. The mechanism here is DBS-induced action potentials can induce synaptic activity and thereby modulating neurotransmitter changes [21]. As a broad definition, neuroplasticity is a phenomenon that causes structural and functional changes to the brain in response to intrinsic and extrinsic stimuli [22].

Given the benefits of DBS that have been investigated in other neurological and psychiatric disorders, one strategy is to conduct more preclinical studies on the efficacy of DBS in ASD. Furthermore, since DBS has an impact on synaptic plasticity, it will be worthwhile to choose an ASD model characterized by dysfunction in synaptic function [13].

1.3 Clinical Targets of Deep Brain Stimulation in Autism Spectrum Disorder

Targets of DBS for ASD have been previously studied and published as case reports. Different targets are being evaluated based on the most predominant symptom of ASD. For instance, nucleus accumbens as a target is currently being investigated in a clinical trial for primarily self-injurious behavior [23]. The children selected for this trial have been refractory to medications and the behavior exhibited is life-threatening. In the future, should DBS ever be indicated for refractory autistic patients, choosing an anatomical target for each patient will be no trivial task, as ASD exists on a spectrum. This will likely depend on the most predominant symptom of ASD and will be highly personalized. Several possibilities are summarized in Table 1.1.

Table 1.1: Summary of clinical DBS targets and the corresponding deficit improved. Of note, amygdala and thalamus were targets more useful for social behavior deficits [9, 24–26].

DBS Targets	**Symptom Improved**
Nucleus Accumbens	Improves Self-Injurious Behavior
Amygdala	Speech and Social Cognition
Globus Pallidus	Improved Stereotypies
Thalamus	Social Behavior Deficit

Several DBS case reports have been conducted in severely autistic patients with targets at the BLA, NAc, and globus pallidus. In one case, debilitating SIB was relieved by stimulating NAc [9].

Table 1.2: Case study in an adolescent male undergoing DBS of nucleus accumbens [9].

Author and Year	**Park et al, 2016** [9]
Age and Sex	14
Sex	Male
Presentation	ASD and SIB resistant to medical and behavioral regimen
DBS Primary Target	Nucleus Accumbens
DBS Parameters	90 μs, 130 Hz, 3 – 5 V
Outcome	Decreased SIB, improved expression and comprehension, decreased T1 cortical density in pre and post central gyrus, supplementary motor cortex, and precuneus (located in superior parietal lobe)
Surgery Specifications	Similar to ventral striatum/ventral capsule DBS for OCD

Case reports in multiple treatment-resistant adolescents have shown that deep brain stimulation (DBS) results in improvements in speech initiation, social cognition, and a decrease in self-injurious behavior with targets at the basolateral amygdala and nucleus accumbens as described in Table 1.2 and Table 1.3 [9, 22]. Particularly, stimulation of the BLA ameliorated symptoms including social deficits and speech initiation in a young adolescent patient [24].

Table 1.3: Case study in an adolescent male undergoing DBS of basolateral amygdala [24].

Author and Year	**Sturm et al, 2012** [24]
Age	13
Sex	Male
Presentation	Kanner syndrome
DBS Primary Target	Basolateral Amygdala
Secondary Targets	Paralaminar Amygdala Central Amygdala Supra-amygdaloid projection system
DBS Parameters	120 μs, 130 Hz, 2 – 6.5 V
Outcome	Improvement in rudimentary speech initiation, nocturnal sleep, social cognition Decrease in self injurious behavior
Surgery Specifications	Two Quadripolar DBS electrodes

Lastly, another two cases explored DBS in the globus pallidus (Table 1.4) for stereotypies and dystonia however in one of the patients, symptoms returned to baseline in 6 months [25].

Table 1.4: Case study in two patients with targets at globus pallidus internus and anterior limb of internal capsule [25].

Author and Year	**Stocco and Baizabal-Carvallo, 2014** [25]	
Age	19	17
Sex	Female	Male
Presentation	Treatment resistant SIB, motor stereotypies, dystonia	Treatment resistant SIB, motor stereotypies, intellectual disability
Genetic Testing	Monosomy 2p and Trisomy 20p	None
DBS Primary Target	Right Globus pallidus internus	Bilateral Globus pallidus internus and bilateral Anterior Limb of Internal Capsule
DBS Parameters	120 μs, 80 Hz, 3.3 V	120 μs, 80 Hz, 2 – 2.5 V
Outcome	Decreased stereotypies and dystonia	Symptoms improved however returned to baseline after 6 months

1.4 Preclinical Targets of Deep Brain Stimulation in Autism Spectrum Disorder

To date, few DBS studies have yet been conducted in animal models of ASD. Preclinical studies have conducted research on the impact of electrical stimulation on neurochemical and behavioral aspects in ASD mouse models. Prior studies of DBS at targets such as the prefrontal cortex, subthalamic nucleus, and central thalamus have shown improvements in autistic mice [26 – 28]. Both clinical and preclinical targets are visualized in Figure 1.2.

In a valproic acid-induced rat model, infralimbic prefrontal cortex was investigated as a targt for high frequency DBS. Here, it was shown that the DBS rats improvement in sociability deficits, and a reduction in axiety and hyperactivity [27]. Another study combined the use of MRI imaging with DBS and found improved magnetic resonance imaging (MRI) signals in the motor cortex, somatosensory cortex, caudate putamen, anterior cingulate cortex, thalamus and hippocampus. Improved social interaction was also seen [26]. Lastly, high frequency DBS at the subthalamic nucleus reduced excessive self-grooming in a Viaat-Mecp2(-/y) and Shank3B(-/-) mouse model [28]. In this study, social interaction did not improve with DBS.

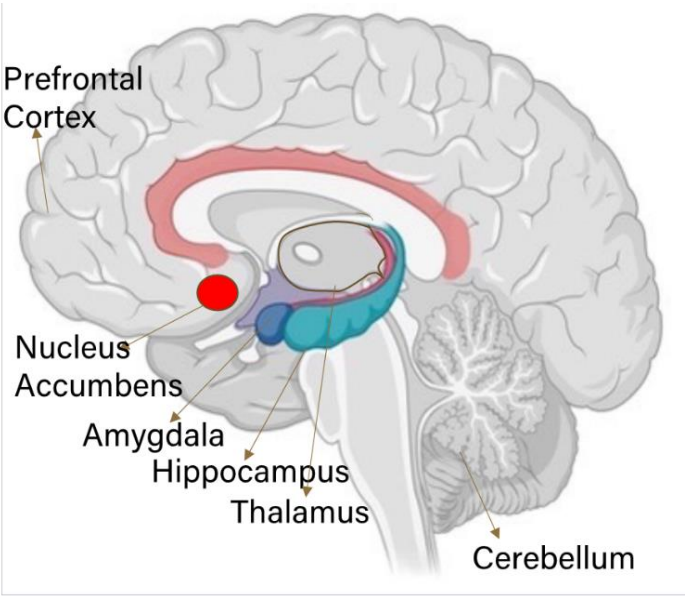

Figure 1.2: Brain regions in humans that are identified as DBS targets in both clinical (nucleus accumbens, and amygdala) and preclinical literature (prefrontal cortex, hippocampus, cerebellum, and thalamus) for ASD [9, 24, 26, 27, 29–31]. Created and adapted from Biorender.com

1.5 Other Approaches of Neuromodulation in ASD

Other forms of clinical neuromodulation strategies explored in ASD include repetitive magnetic stimulation (rTMS) [32], vagal nerve stimulation (VNS) [33], and electroconvulsive therapy (ECT) [34]. ECT is employed for severe and refractory SIB and is administered in combination with antidepressants. However, the drawback is it needs to be administered once every five days. DBS on the other hand requires weekly visits initially and then monthly visits, the goal of which is to achieve optimal parameter settings [35]. rTMS seems to be a promising approach as a clinical trial demonstrated stimulation at medial prefrontal cortex improved social impairment and anxiety [32, 34]. rTMS also has another disadvantage of side effects such as headaches and facial twitching [32, 36].

1.6 Mouse model of *Syngap1*$^{+/-}$ haploinsufficiency

We employed a mouse model of *Syngap1*$^{+/-}$ haploinsufficiency that causes an increase in α-amino-3-hydroxy-5-methyl-4-isoxazolepropionic acid (AMPA) receptors trafficking due to decreased regulation by SynGAP1 protein [37]. The haploinsufficient model results in only one functional gene, thereby either less protein is available or truncated protein variants are produced [37]. SynGAP1 mRNA and protein content is highly expressed in the brain and is primarily found in the forebrain, such as the cortex, hippocampus, and olfactory bulb. SynGAP1 is a GTPase activating protein found in the postsynaptic density and is highly found in dendritic spines [37, 38]. The *Syngap1*$^{+/-}$ haploinsufficient model causes several pathologies such as intellectual disability (ID), ASD and epilepsy. Homozygous animals do not survive beyond the perinatal phase, or death a few days after birth [37].

The primary function of the SynGAP1 protein is to maintain long-term potentiation (LTP) through N-methyl-D-aspartate (NMDA) receptors and AMPA receptor insertion [37]. SynGAP1 is initially localized in the cytosol, and after post-natal day 14 (P14) is primarily found in post-synaptic density (PSD) [37, 39, 40]. In addition, aberration of SynGAP1 protein results in stubby spines in the dendrites and occlusion of LTP [37, 40].

At the molecular level in the hippocampus, altered dendritic spines result in ‘mushroom-shaped spines – ’this is a morphological feature present in Fragile X Messenger Ribonucleoprotein 1 (*Fmr1)* mutant mice as well (an ASD mouse model) and implicates microanatomical pathology

that is shared across genetic variants in autism [13]. Moreover, metabotropic glutamate receptor 5 (mGluR5), Ras, and ERK 1/2 phosphorylation pathways are elevated in *Fmr1*$^{-/y}$ with, Ras and extracellular signal-regulated kinase (ERK) phosphorylation pronounced in *Syngap1*$^{+/-}$. This eventually causes elevated basal protein synthesis in the hippocampus [41]. This elevated protein synthesis present in heterozygous models eventually causes mGluR-dependent long-term depression (LTD) [42]. LTD is a process where there is 'long-lasting and activity-dependent decreased synaptic efficacy' [43].

Convergence of these multiple autism risk genes is displayed in Figure 1.3. Therefore, this convergence suggests by selecting one genetic mutation model, our findings can be translated to other common autism risk genes models as well. These include proteins include SHANK3, neuroligins, and in Fragile X Messenger Ribonucleoprotein 1 (FMRP) [12, 44, 45].

Although these synaptic changes seem permanent, the latest scientific discourse has shown pharmacological agents and neuromodulation techniques rescue autistic features beyond the critical period of plasticity [37, 38, 46, 47]. Adult restoration of SynGAP1 protein previously restored long-term contextual memory deficits. In this study, increased theta oscillations were also found [37]. Even though these studies are promising, the question remains whether re-expression can be translated to human patients.

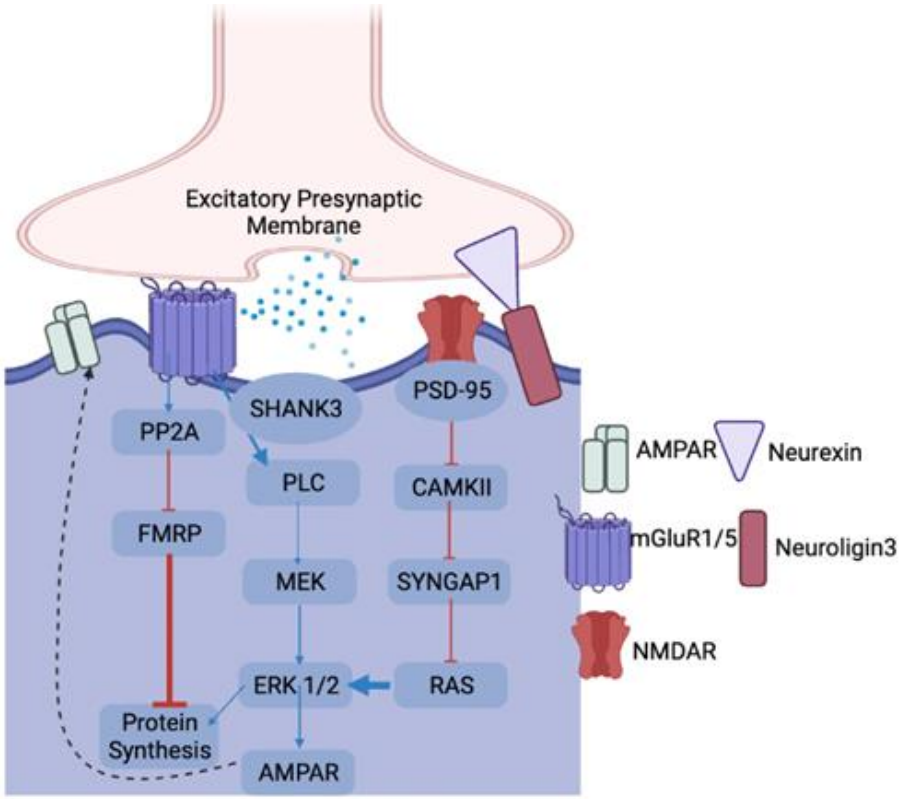

Figure 1.3: Convergence of synaptic pathways in the post-synaptic density [13]. PP2A: Protein phosphatase 2; FMRP: fragile X mental retardation protein; PLC: phospholipase C; MEK: Mitogen-activated protein kinase kinase; ERK: Extracellular signal-regulated kinase; AMPAR: α-amino-3-hydroxy-5-methyl-4-isoxazolepropionic acid receptor; PSD-95: Postsynaptic density protein 95; CaMKII: Calcium/calmodulin-dependent protein kinase II; NMDAR: N-methyl-D-aspartate (NMDA) receptor
Created and adapted in Biorender.com

1.7 Basolateral Amygdala as a Target for DBS in the SynGAP model

At the anatomical level, the BLA serves as a channel between central and superficial nuclei – each nuclei has further connections with targets such as the hypothalamus, thalamus, reticular formation, and lateral olfactory target [48, 49]. Studies in humans have shown an increased amygdalar thickness in ASD [50]. In addition, amygdalar lesions result in pathological phenomena such as abnormal fear processing, abnormal fear-based memory, and failure to maintain eye contact [48].

BLA serves as a potential target for DBS in autistic mice, due to its fiber tract connections to the prefrontal cortex, hippocampus, motor cortex, sensory cortex, and the thalamus [10, 51]. These are desirable connections as these regions are heavily affected in ASD patients [10, 52]. Therefore, the hypothesis is that BLA stimulation will improve deficits in these regions.

BLA aberrations are identified in many genetic variants of ASD such as in *Syngap1*$^{+/-}$ haploinsufficiency, valproic acid model of ASD, and in the (fragile X messenger ribonucleoprotein 1) *fmr1* model [27, 53]. Interestingly, this region is also associated with anomalies in fear conditioning and social interactions [53]. We thereby studied the therapeutic benefits of stimulation, record LFPs at BLA and the resulting behavioral phenotype.

Previous research has established that the basolateral amygdala is also involved with establishing declarative memory. Here, it was found that stimulating the BLA at 50 Hz and 8 Hz, resulted in theta waves in hippocampus. These theta waves in particular appear during cognitive tasks in rodents, and have been demonstrated to be associated with episodic memory [54]. Frequency at 50 Hz correlates well with gamma waves, while frequency at 8 Hz correlates with theta waves [55].

Furthermore, recent work on rat basal amygdala found increase excitability in *Syngap1*$^{+/-}$, as well as a deficit in LTP from thalamic input [45]. Considering autism risk genes have significant implications at BLA, we wish to study this target in more depth.

Hence, we have considered electrophysiological and anatomical connection between BLA and hippocampus – the key area of *Syngap1*$^{+/-}$ pathophysiology. Therefore, our central hypothesis is that stimulation at the BLA will ameliorate the behavioral deficits in *Syngap1*$^{+/-}$ mice and will result in neuroplasticity.

2. OPTIMIZATION OF THE CHRONIC DEEP BRAIN STIMULATION SURGERY PROTOCOL IN THE SYNGAP1+/- MOUSE MODEL

2.1 Introduction

Expertise and knowledge of chronic surgeries in rodents is essential for success in complex stereotaxic surgeries. Ensuring appropriate surgical steps and protocols is essential to ensure any removal of confounding variables such as ensuring there are no infections, or added stress to mice with inappropriate handling [56]. If techniques are not appropriately followed, they can result in unknown variables that can adversely impact the scientific questions and outcomes being addressed. Deep brain stimulation surgeries present an added layer of complexity to rodent surgeries [57]. Homeostasis must also be additionally maintained within the cranial cavity in addition to the rest of the steps. A much higher margin of error is present while performing stereotaxic surgeries in mice, considering mouse brains are much smaller in comparison with rats and monkeys. Therefore, in addition to accurate placement of electrodes during the surgery itself, it is essential to conduct histology to determine correct electrode implantation within the BLA. Herein, we present optimization of chronic DBS surgery in the *Syngap1+/-* mouse model using stereotaxic coordinates that target the BLA. Following optimization, we ensured acquisition of raw electrophysiological signals from chronically-implanted mice.

2.2 Methods

2.2.1 Subjects

Mouse colonies of heterozygous and homozygous *Syngap*^{1tm1Rlh} were maintained from the Jackson Laboratory. Breeding was continued in accordance with the Jackson Laboratory Manual. These mice underwent timed mating and pups were weaned at 21 days. Our experiments were initially focused on 60-day old mice – however after considering anesthesia differences, I gravitated towards accomplishing these experiments in adult models of mice of age 3 – 4 months. Mice of each respective sex were housed separately, with each cage containing 2 to 5 mice per cage. However, following electrode implantation, mice were singly-housed to avoid injuries associated when other mice tend to remove the electrodes. All procedures in mice were carried out

in accordance with Purdue Animal Care and Use Committee (PACUC) under the protocol numbers 1801001682 and 2004002031.

2.2.2 Identification of Heterozygous and Wildtype Mouse using Genotyping

Our study employed the *Syngap1*$^{+/-}$ haploinsufficient mouse model where a litter is comprised of both heterozygous and the wildtype pups. . Therefore, following breeding of mice, they were genotyped to identify heterozygous (ASD phenotype) or wildtype (neurotypical control) mice. Mice underwent ear notching for both identification and genotyping purposes. This was a significant step that required careful processing of samples so bands are accurately identified and errors in identification of heterozygous and wildtype mice do not occur.

Briefly, ear notching was done using ear punch (Fine Science Tools). Samples are collected for which polymerase chain reaction is completed. Gels are then run at 110 V for 50 – 60 min and imaged on Azure UV 305. One band is obtained at for wildtype at 300 bp, and heterozygous will yield two bands at 463bp and 300bp [58, 59].

2.2.3 Overview of the DBS Surgical Technique

Two consecutive surgeries were performed in all heterozygous and wildtype mice. The first headplate surgery was performed at least 3 days earlier to the burr hole surgery for electrode implantation. Burr holes were then drilled bilaterally for the second surgery. The headplate surgery was conducted to ensure the mouse's head is stabilized during neural recordings.

2.2.4 Headplate Surgery

A full circular headplate made of titanium with an 8 mm diameter was implanted centered on bregma (Figure 2.1). This is to prevent errors in stereotaxic implantation of electrodes. In addition, the headplate provides stability during electrode implantation and subsequent stimulation. The surgery was done in accordance with previously published protocols [60].

Briefly, mice in the age group of 3 to 4 months underwent two surgical procedures. The groups were balanced for male and female mice, as well as for heterozygous and wildtype mice. Mice were induced at 3% isoflurane at 0.9 flow rate of oxygen. They were then maintained at 1.75 % — 2.25 % isoflurane and placed on a heating pad during surgery. A cutaneous injection of

lidocaine (0.03 mL; 2% lidocaine; 1:10 dilution) was given at the surgical site to reduce pain. Meloxicam (10 mg/kg) was given subcutaneously. The head was kept affixed by inserting ear bars at an angle.

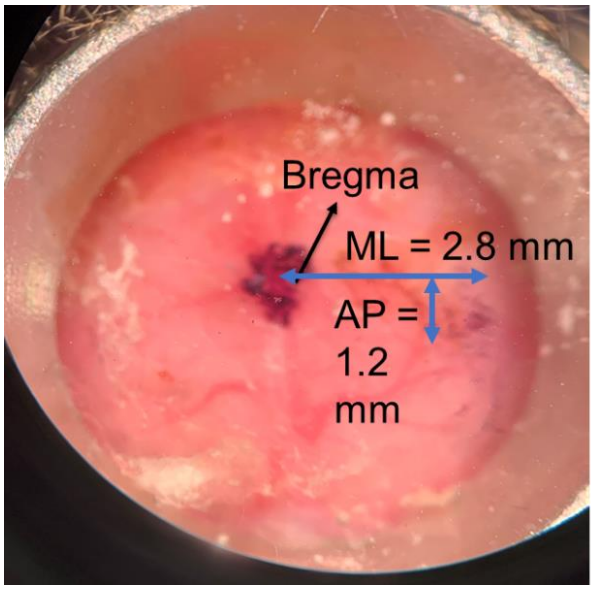

Figure 2.1: A headplated mouse skull is shown. Bregma is represented by a black marker and site of right BLA coordinates marked by red circle. The mediolateral (ML) and anteroposterior (AP) coordinates are shown.

After a flap of skin was cut directly at the surgical site, saline was used to continuously irrigate the site. Following surgical incision, the membrane and connective tissue over the skull were separated. Ligaments and muscles attached to the skull were gently separated using forceps, to create pockets for dental cement to settle in. Aseptic techniques and surgical instruments (Fine Science Tools) sterilized in a hot-bead sterilizer were used throughout.

The surface of the skull was then gently scraped with a curette to promote adhesion of the dental cement (Metabond; Parkell) to the skull. The cranial sutures were carefully avoided during scraping to prevent bleeding. Before applying Metabond, bregma was marked by a permanent pen. A layer of radiolucent Metabond was then gently applied at the surgical site, and the headplate quickly affixed. Additionally, after performing a number of trial surgeries, the site for implantation of the stimulation electrodes was easily identified as it passes through two vessels running laterally (Figure 2.1).

Throughout the surgery, the mice were monitored for breathing rate, toe reflex, and color of membranes and toes. Once the surgery was completed, we modified the post-operative recovery

phase by allowing these mice to be on oxygen without isoflurane and with additional support by keeping them on heating pads.

2.2.5 Choosing Electrode Placement by using a Stereotaxic Atlas

Preparation of the craniotomy entails ensuring appropriate coordinates by verification from a corresponding stereotaxic atlas. To target electrode implantation into the BLA structure, we identified the coordinates using a Mouse Atlas (Paxinos and Franklin's The Mouse Brain in Stereotaxic Coordinates) that has detailed brain cross-sections for mice aged at 3 months with a weight of 26-30 g. The coordinates for BLA will be adapted from this atlas: anteroposterior (AP)= −1.2 mm, mediolateral (ML)= ±2.8 mm, dorsoventral (DV)= −4.8 mm (Figure 2.2).

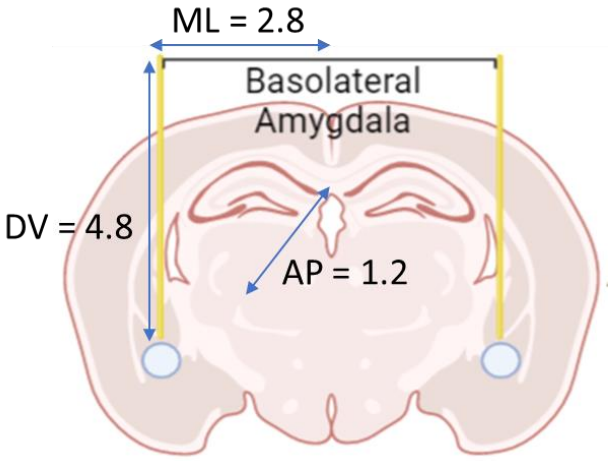

Figure 2.2: Representation of stereotaxis brain coordinates that employed in the mice model. In the training phase, unilateral implantation was completed. Bilateral implantation was completed for ongoing behavior experiments. Created and adapted in Biorender.com

2.2.6 Soldering Ground Electrodes

Since unipolar electrodes were used for stimulation, we additionally had to implant a ground electrode to complete the electrical circuit. We used custom-made ground electrodes, created by soldering silver wire to gold connectors. Lead solder was melted on top of the silver wire and gold connectors. Careful consideration was given to ensure the electrode produced as a result was taut and secure, to prevent any breakage of the electrode during the craniotomy. The ground electrodes were then lowered down in their respective burr hole so they could provide a conductive electrical pathway.

2.2.7 Tungsten Electrodes for Stimulation and Recordings

For our pilot project, our stimulating electrodes were made of tungsten and were implanted on the right side at basolateral amygdala. These electrodes were unipolar with a diameter of 75 µm and length of 1.5 cm. The impedance of these electrodes was 0.1 MOhm. The tapered exposed tip is essential to ensure minimal damage while inserting the electrode and had a diameter of 2 µm. These electrodes allow for multi-unit recordings and stimulation. Figure 2.3 shows a schematic of the electrode, with the insulated layer of parylene-C clearly represented.

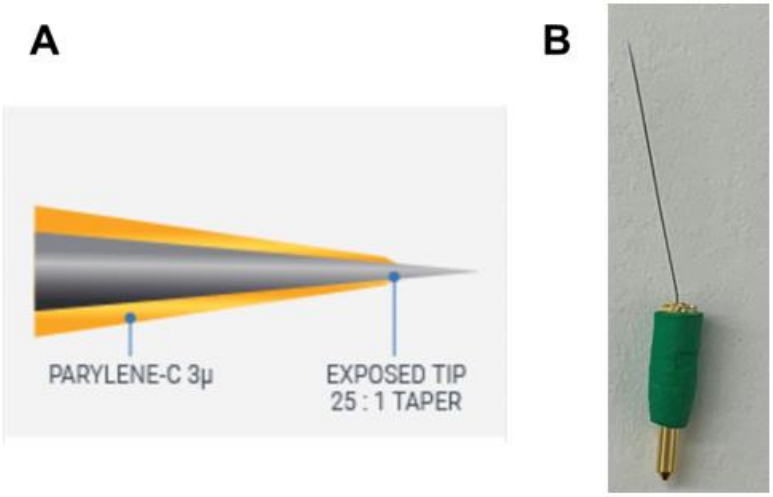

Figure 2.3: A) Schematic of a tungsten electrode. B) 1.5 cm tungsten electrode with gold connector covered in green cover. Picture reprinted with permission from Microprobes for Life Science, Inc [61].

2.2.8 Surgery for Electrode Implantation

The goal of this surgery is to place two electrodes at the right and left basolateral amygdala. After administration of anesthesia, linear tungsten electrodes (Microprobes Life Sciences) were inserted bilaterally at the coordinates using a micromanipulator (Sutter Instruments MPC-200/MPC-385).

As described for the headplate surgery, mice were first induced at 3% isoflurane and 0.9 flow rate of oxygen. They were then maintained at 1.75% – 2.25%. Meloxicam (10 mg/kg) and dexamethasone (10 mg/kg) were administered subcutaneously to reduce pain and inflammation in the brain. Toe reflexes and the color of mucus membranes were continuously monitored to ensure proper anesthetic depth of the animal. The head was affixed using appropriate screws on the

headplate. This ensured there was no movement of the head throughout the surgery, and accurate marking of stereotaxic coordinates (Figure 2.4). Careful consideration must be given at this step, as inappropriate traction can loosen the headplate.

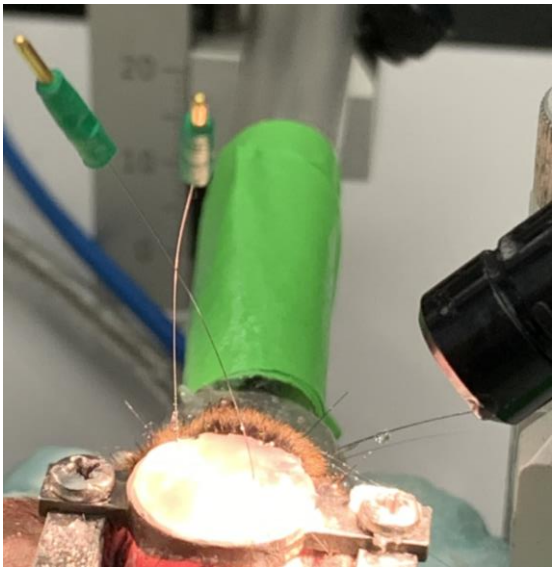

Figure 2.4: Demonstration of headplate affixed during stereotaxic surgery. The affixed headplate is essential for the actual surgery and for performing the *in vivo* electrophysiology experiments.

The first step of the surgery was to mark out the right and left basolateral amygdala coordinates. This was achieved by placing the micromanipulator directly above first the bregma and the electrode descended. To do so, an electrode was positioned just above bregma. Next, coordinates were set to 0 on the Digital Stereotaxic screen (Figure 2.5). The ML and AP on both sides were determined at this step under an angled microscope. A dental drill was used to drill the Metabond until the skull was visualized. Surgery site was continuously irrigated with saline to prevent any damage to the brain due to the heat generated. As vessels became more clearly visible while reaching the surface, thawed artificial cerebrospinal fluid (stored at -4 °C) was irrigated.

Figure 2.5: Coordinates were selected on Stoelting Digital Stereotaxic System as shown

A total of 3 burr holes were then made: two at the bilateral BLA sites and one is at the ground electrode site. The micromanipulator was once again adjusted to verify the ML and AP electrode location. Adjustments to the burr hole were made if not at the correct location, and the drilling of the circular burr hole was extended.

The electrode was then descended in the burr hole site (Figure 2.4), and the site is cleared out using a dental tip. Once the brain was visualized under the microscope, the dorsoventral coordinates were set to 0, and descended to 4.8 mm.

Kwik-sil was added to each site to hold the electrode, and a small layer of metabond was applied on top of the Kwik-sil. Kwik-sil is a silicon elastomer that is biocompatible with the tissue in the brain.

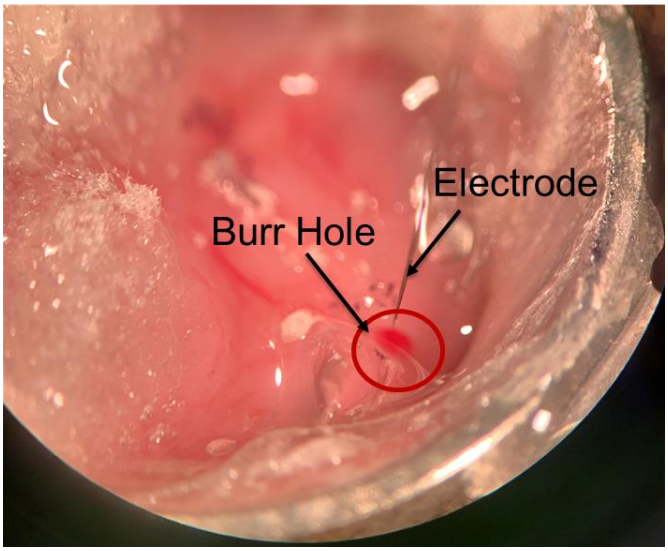

Figure 2.6: Demonstration of an electrode implantation surgery. Here, an electrode is being descended at the site with aid of the dorsoventral coordinates selection on the digital stereotaxic system

Lastly the ground electrode was descended at the site, but it did not penetrate the cortical surface (Figure 2.6). Again, the site was covered with Kwik-sil and then with metabond. Once dried within a few seconds, all wires were gently wrapped in a mixture of acrylic powder and cyanoacrylate. Electrode wires must be carefully secured to ensure that the mice do not tug or pull on these wires. The connectors must remain exposed.

The total duration of the surgery can vary from 2 to 3 hours – therefore to ensure adequate recovery, mice are kept under oxygen without isoflurane on a heated pad to promote recovery. Mice are then monitored during the post-surgical recovery phase.

2.2.9 Post-Surgical Care of Mice

Mice were monitored for at least 2 days by research personnel to ensure there were no signs of pain or discomfort. For each headplate surgery, Meloxicam was administered for two days post-operatively. For each electrode implantation surgery, Meloxicam (10 mg/kg) and Dexamethasone (10mg/kg) were administered post-operatively.

Mice with obvious signs of discomfort were excluded from analysis and were subsequently euthanized if pain management did not improve their condition. Mice whose headplate got dislocated following surgeries were also euthanized.

2.2.10 Histological Verification

Methods of histological verification of electrode placement were modified from previous literature [43, 49]. Briefly, histological analysis using both hematoxylin and eosin staining was be used to verify the precise stereotaxic coordinates after passing an anodal current 30 µA for 10 seconds.

Mice were first euthanized using isoflurane administered at 5%. Once the mucous membranes were pale, and breathing had ceased, the headplate was adjusted and screwed down on the electrophysiological apparatus.

After attaching connectors of the corresponding channels on the 18-pin wire adapter, impedance values were assessed. Verification of channels with impedance values in the range of 0-300 were selected. Here, stimulation pulses were provided for 1 second on and then 1 second off phase in order to lesion the brain at the site of the electrode tip. A total of 10 trials were stimulation to lesion at the area. We used anodal current at 30 µA, 130 Hz, level triggered, biphasic pulses.

Once stimulation for the purposes of lesioning was completed, we ensured euthanasia by cervical dislocation. Next, the headplate was carefully removed so as not to cause any damage the brain given the fragile state of the mouse skull. If the headplate is not removed appropriately, the underlying dental cement can damage the brain surface underneath.

Once the skull was exposed, dissection of brain was completed by first traversing through the cervical muscles. Fine scissors were then used to cut the skull at the occiput – traversing through the sagittal suture passing lambda and bregma. Transverse cuts were then given at the skull in a crisscross fashion, and the 4 pieces of skull were then removed by forceps. A spatula was then used to gently remove the intact brain from the skullbase. The brain specimens were immediately preserved in 4% of paraformaldehyde in PBS.

2.3 Results

2.3.1 Optimization of Electrode Implantation for DBS in Mice

Trial experiments were performed in the training group to ensure optimization of the electrode implantation surgery. Electrode configurations included unipolar vs bipolar, and size of electrodes was determined. These strategies are summarized in Table 2.1.

Furthermore, we conducted craniotomies with bilateral implants without ground electrodes (n = 3). The idea behind this was whether an electrode implanted deep in the brain can act as a ground electrode. For instance, we tested if we could attain recordings from right BLA while grounding left BLA.

Importantly, no discernible signals were achieved, and instead noisy data was attained. Therefore, we verified the importance of placing a silver ground electrode close to the surface of the cortex without probing the brain.

Table 2.1: Optimization strategies of electrode parameters in addition to the final specifications. The strategies included selecting unipolar electrode, optimizing electrode length, and choosing the right material for stimulation.

Optimization Strategy	**Electrode Specifications**
Unipolar vs Bipolar	• Unipolar was selected considering greater efficacy based on previous literature and due to wider stimulation in space [62]
Electrode Length	• We started out with a standard 3-inch electrode length – importantly clipping the electrodes is an ineffective strategy considering the tapered end is removed • Furthermore, in many surgeries, traction of a longer wire resulted in electrodes to slip out and therefore the results of these surgeries were discarded from the analysis • Therefore, a customized electrode length of 1.5 cm was more applicable
Material of Electrode	• Tungsten electrodes were used for their applicability in chronic stimulation, along with durability • The major drawback is tungsten electrodes are inferior to platinum/iridium electrodes as tungsten electrodes have a higher likelihood of corrosion [63] • For our exploratory study, tunsgsten electrodes were more useful due to a lower cost

2.3.2 Differences in Anesthesia Management between wildtype and *Syngap1*$^{+/-}$ mice

Heterozygous mice, that is the mice carrying only one functional copy of *Syngap1* and displaying the ASD phenotype, were noted to have heightened sensations, hyperactivity, and aggressive behavior towards other mice in the same cage. It was also noted that the heterozygous mice in comparison with wildtype were less responsive to isoflurane anesthesia. Importantly, many

of these mice were susceptible to any subcutaneous injections despite being on maintenance anesthesia at the start of the surgery. They also took time for the toe reflex to go down. These differences are shown in Figure 2.7.

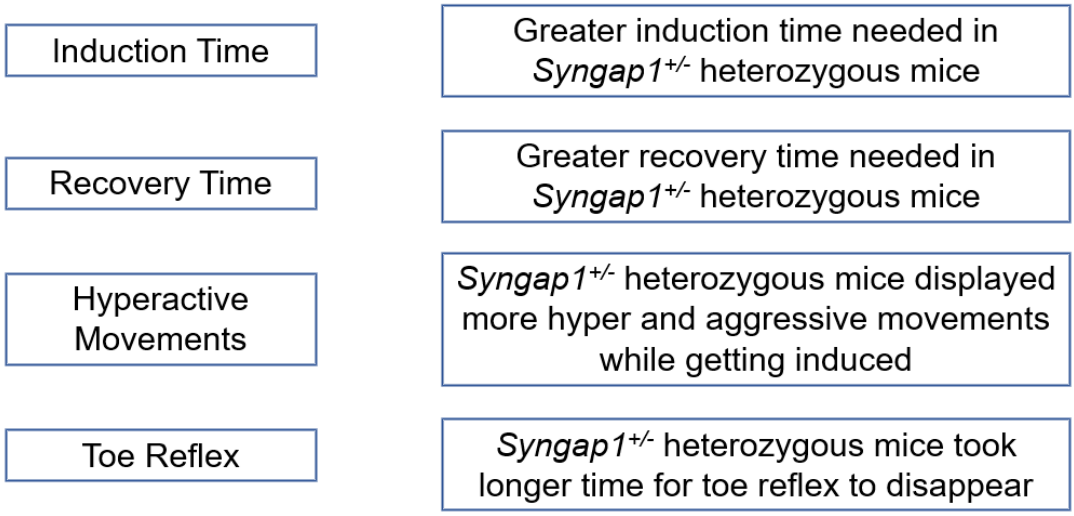

Figure 2.7: Anesthetic differences between heterozygous and wildtype mice with relation to isoflurane anesthesia. Of note, heterozygous mice took a longer time to anesthetize, showed more hyper movements, and took a longer time for their toe reflex to disappear. Implementing changes due to these differences can help ensure recovery.

With experience, I found that the most effective strategy for heterozygous mice was to reduce isoflurane anesthesia with caution. Importantly, after the induction phase ended an effective strategy was to gradually reduce the anesthesia from 2.75% to 2.5% to 2.25% until the toe reflex completely disappeared. Few heterozygous mice were maintained at 2% isoflurane, whereas wildtype mice could be brought down to 1.75% isoflurane. In addition, breathing rate was monitored to ensure a second gap was present between the breaths. If there are only a couple breaths per minute, then the mouse has respiratory depression, and the anesthesia must be reduced. This must be done in increments though, as heterozygous mice can develop a toe reflex if isoflurane is drastically reduced. Finally, the surgery time must be kept short for these mice, and such a strategy improved with the researcher's experience in performing surgeries. These strategies are summarized in Figure 2.8.

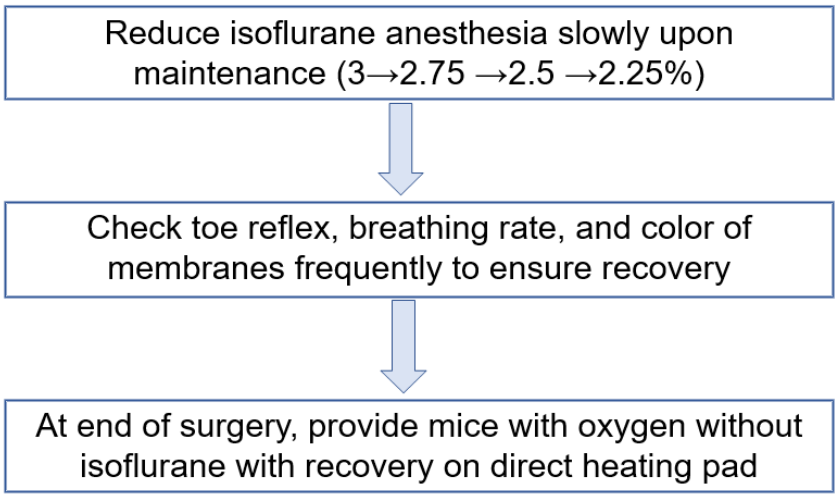

Figure 2.8: Anesthetic strategies that were useful for ensuring recovery in heterozygous mice

Unfortunately, many of these mice did not survive during the surgery or died in the immediate recovery phase — to circumvent this we ensured recovery of mice directly on a heating pad once the surgery commenced. The heating pad had a closer contact to the mouse with only a thin drape separating to provide more direct heat to the mouse. Oxygen was given without isoflurane until breathing normalized.

2.3.3 Lesioning shown at BLA coordinates through Histological Slices confirming Electrodes

To collect brains for histology the *Syngap1*$^{+/-}$ mice were first euthanized with 5% isoflurane anesthesia [30, 64]. This was an essential step provided *Syngap1*$^{+/-}$ mice reacted in terms of faster behavioral response to higher amplitude currents of 15 µA. Coronal sections and staining of brains were carried out by the histology core and are shown in Figure 2.9.

These are the first set of mice brains that did not show lesioning. For future experiments, lesioning parameters should be optimized so only single pulses without a charge resting phase is given to lesion [30].

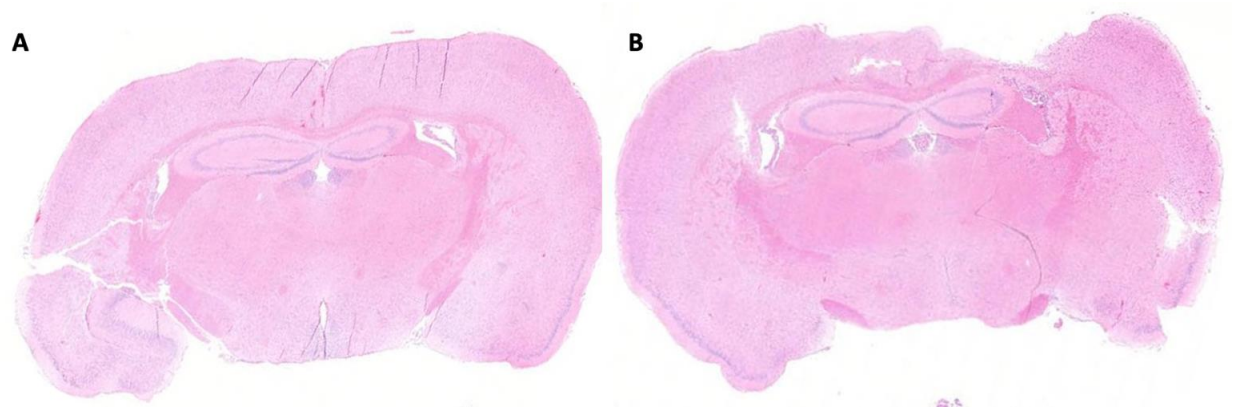

Figure 2.9: **A)** Control mice that did not undergo surgery stained on H&E **B)** Stimulated brains on the right side of the brain hemisphere

2.4 Conclusions

Taken together, I worked on a model of DBS that can be translated to other neurodevelopmental disorders rodent models. Most importantly, recovery of mice was emphasized to ensure testing of animals for subsequent weeks. This model can further be used for electrophysiological analysis, behavioral analysis, and proteomics. Furthermore, anesthetic differences were consistently noticed in *Syngap1*$^{+/-}$ mice, which were also previously noted in Shank3$^{+/\Delta C}$ mutation mice models. While at present we are not certain of the differences in receptors that caused such a change in *Syngap1*$^{+/-}$ mice in the Shank3$^{+/\Delta C}$ mutation mice models differences in NR1 (a subunit of NMDA receptor) and PSD95 was noted to be the reason [65]. In addition, human patients with autism are also well-known to have disturbances in sensory processing [10]. Moreover, a workflow was established to accurately place electrodes and to verify the coordinates histologically at BLA.

3. LOCAL FIELD POTENTIALS AT THE BASOLATERAL AMYGDALA IN THE *SYNGAP1*$^{+/-}$ MODEL AS A RESULT OF DEEP BRAIN STIMULATION

3.1 Introduction

The amygdala is located in the medial temporal lobe in the human brain bilaterally. It is a well-connected structure with other parts of the brain, as detailed in the Introduction chapter. Additionally, the amygdala has several subdivisions including the cortical and medial nuclei, central nucleus, and the basolateral complex. Apart from the projections of BLA to other parts of the brain, there are also extensive intrinsic connections of the basolateral complex with other amygdalar nuclei [66, 67].

Electrophysiological correlation can provide us with greater insight to the frequencies associated with BLA. Since we are implanting the electrodes deep in the nucleus, the resulting oscillations are called local field potentials (LFPs). Specifically, LFPs are an aggregate low-frequency activity of extracellular field potentials [68]. Previous literature has characteristically concentrated on low frequency LFPs in the range of 1 – 50 Hz, and high frequency oscillations in the range of 50-100 Hz [69]. The frequency content of various frequencies include delta (0.1 – 3.5 Hz), theta (4 – 8 Hz), alpha (8 – 12 Hz), beta (12 – 35 Hz), and gamma (35 – 80 Hz) [68–70].

These complex oscillations have been described in the previous literature that vary with the state the rodent is in. Additionally, while the BLA has traditionally been associated with fear-based emotional and associative learning, more research has pointed towards BLA's function in declarative memory. Previous literature showed 50/8 Hz modulation elicited theta-gamma modulation in the hippocampus essential for forming memories [55]. Furthermore, it has been demonstrated that in states of fear, theta oscillations dominate in BLA, hippocampus, and medial prefrontal cortex. On the contrary, during the state of safety this got converted to fast gamma waves. Lastly, in a state of an expected reward slow gamma waves were present [70, 71].

An important component of my experiments was to assess the optimal DBS parameters. DBS traditional parameters for Parkinsonian disorder are well-established in literature as chronic unipolar stimulation, 2.5–3.5 V, impulse duration 60–90 μs, and frequency 130–180 Hz [72]. However, currently studies on DBS parameters for psychiatric disorders are still ongoing [73]. Furthermore, it is not known whether DBS parameters for Parkinson's and psychiatric disorders

can be applied to ASD. To mitigate this, we conducted our own trials of stimulation. Briefly, we first selected high frequency pulses of 130 Hz. High frequency stimulation has been known to benefit tremors in Parkinsonian disorder, therefore we carried on with this hypothesis [17]. Pulse width was selected as 100 μs. Lastly, amplitude was selected as 10 μA or 15 μA. The goal is to attain a 'therapeutic window' when selecting the optimal DBS parameters [73].

Briefly, as an exploratory study, we have compared analysis on recordings from BLA pre and post stimulation in heterozygous and wildtype mice. Our primary goal is to assess the frequency content of these oscillations at the BLA. Additionally, I have selected the optimal stimulation parameters for *Syngap1*$^{+/-}$ mice.

3.2 Methods

3.2.1 Testing electrodes in Saline and Impedance Measurements

Before recording from the chronically-implanted electrodes in mice, multiple tests were run to check the appropriate channels and connectors attached to an 18-pin wire adapter (Intan Technologies). This is then connected with an RHS stimulation/recording headstage (Intan Technologies) that has a capacity for 16 channels. Optimization was then completed to check for the correct set of electrodes. In most cases impedance was lowest in channel 5 (~10 kΩ) and carried minimal noise.

3.2.2 Recording Protocol

The mouse was first head-fixed using screws that attach to the headplate on the electrophysiological rig (Figure 3.1). The mice were awake and freely moving. A repeat testing of impedance was completed. Impedance values were <100 kΩ once connectors were placed over the mouse's electrodes. In most cases, this turned out to be channel 5 that had lower impedance compared to other channels. Two minutes of baseline recordings were completed before we started with DBS stimulation.

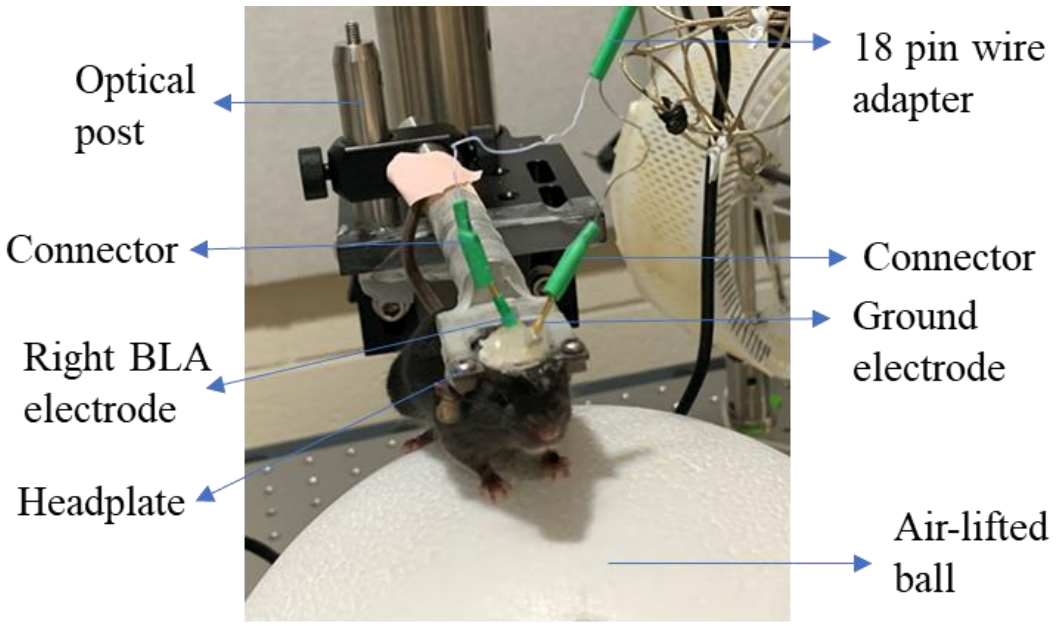

Figure 3.1: Mice are head-fixed on an air lifted ball, that allows them to freely move, and prevents dislocation of the headplate. The stimulating/recording electrode along with the connectors are clearly represented. In addition, the connectors are then attached to the 18-pin wire adapter. This apparatus is used for both recording and stimulation.

3.2.3 Stimulation Protocol

Trials were run for optimal DBS parameters using the behavior observed from the mouse as a metric such as faster running, eye twitching, and tail movements. The goal here is to ensure minimal motor movements are observed in the mice to make stimulation comfortable. However, the amplitude current must not be too low that it does not achieve a therapeutic response. In addition, since we used the Intan Data Acquisition system, we ensured appropriate stimulation setting were used in the interface. Based on observations from further optimizations and behavioral observations our final DBS parameters were 130 Hz, 10 to 15 µA, 100 µs, biphasic square pulse. The trigger settings were level triggered and triggered on low. Specifically, selecting a level triggered option results in the stimulation sequence to deliver given the trigger source (Arduino) remains active. We then chose ‘triggered on low’ setting that allows DBS to be given continuously without the need of pressing a key or giving other input. These triggers were linked to an Arduino that connected to Intan RHS Stimulation/Recording Controller (Figure 3.2). Raw signals that are displayed can then be saved as RHS file that are compatible with MATLAB.

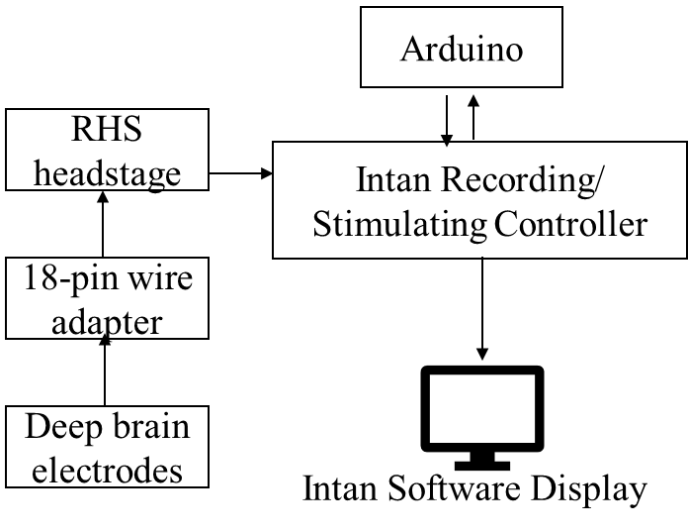

Figure 3.2: A schematic is represented of how the electrodes are eventually connected with the equipment to provide raw signals on screen. First each of the deep brain stimulation electrodes are connected with connectors that are soldered to an 18-pin wire adapter. The 18-pin wire adapter then connects to an RHS headstage (Intan). This is then relayed to the Intan Recording/Stimulating Controller which then provides an output in the form of raw signals on the Intan Data Acquisition Software.

Additionally, 100 trials were run in our pilot group of mice. Each of these trials comprised of 1 second of stimulation, and then 2 seconds of rest phase. Therefore, I ran one set of 100 trials with 10 µA (130 Hz, 100 µs, biphasic square pulse) as displayed in Figure 3.3.

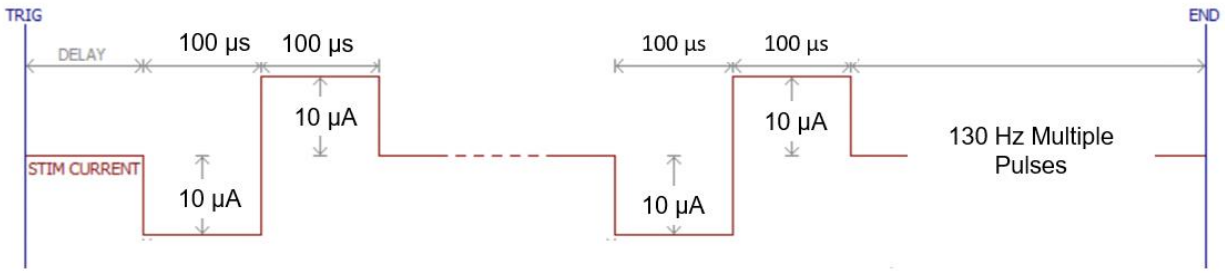

Figure 3.3: A schematic is represented of the first stimulation trial with 10 µA. Here, two pulses are displayed with the following DBS parameters: 130 Hz, 100 µs, and 10 µA. Picture adapted with permission from Intan Technologies [74]

We also ran another set of 100 trials with 15 µA (130 Hz, 100 µs, biphasic square pulse) as displayed in Figure 3.3. Though the data is not shown, we noticed our mice (in both heterozygous and wildtype) were running much faster in the trial with amplitude current of 15 µA. Overall, mice of both heterozygous and wildtype mice were much calmer as assessed by handling following stimulation. However, formal tests of these observations were not run.

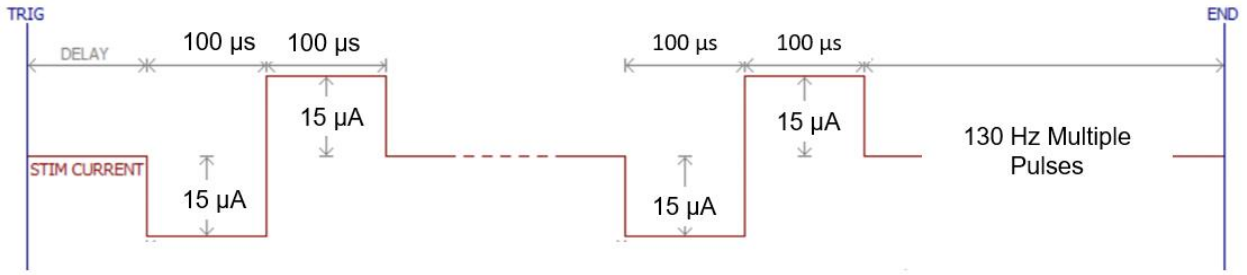

Figure 3.4: A schematic is represented of the second stimulation trial with 15 µA. . Here, two pulses are displayed with the following DBS parameters: 130 Hz, 100 µs, and 15 µA. Picture adapted with permission from Intan Technologies [74]

Furthermore, when traditional DBS parameters (this denotes a high amplitude current) were used we noticed an overt behavioral response to stimulation at 30 µA. The responses included running towards the right side (in a right BLA implantation), eye twitching and movement of the mouse's tail. To keep the stimulation level safe and comfortable for the mice, we ensured such trials were only administered as a single pulse (Figure 3.5).

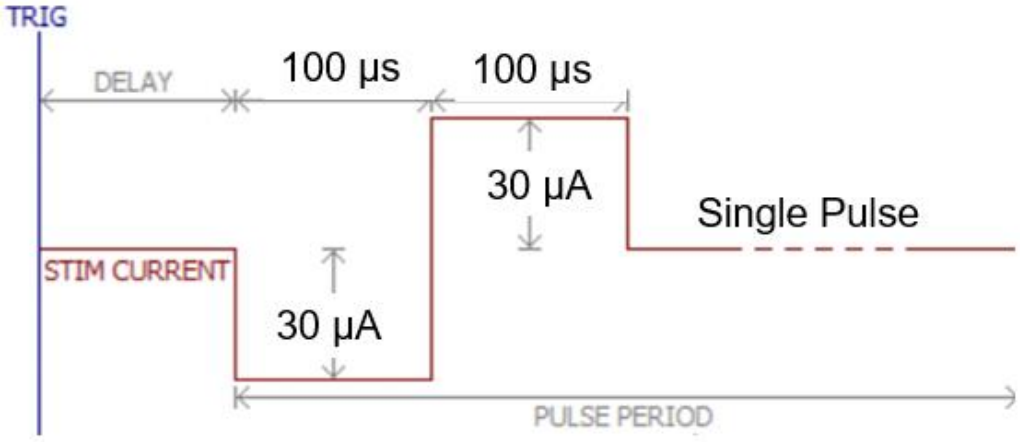

Figure 3.5: An example of trials of stimulation that demonstrated these mice were not responding well to a higher current amplitude. Here, a single pulse was delivered to assess the mouse's behavior in response to stimulation – the parameters were therefore 15 µA, 100 µs, and biphasic single pulse. Picture adapted with permission from Intan Technologies [74].

3.2.4 Signal Processing to generate Local Field Potentials

The goal of signal processing was to ensure that each of the trials were delineated. These signals are already amplified and digitized as they are recorded by Intan. Specifically, the amplifier

bandwidth was between 1.17 Hz – 7.60 kHz. Some of the filtering process can also be done with Intan. Here, we employed a 60 Hz Notch filter to eliminate noise. The notch filter assisted in visualizing raw signals in time and in addition, this filter was saved within the data files as well for analysis. Further filtering was done using a bessel filter with 2 filters and a cut-off frequency of 250 Hz. Bessel filters are analog low pass filters that give out a constant group delay and therefore an optimized transient response [75].

These raw signals and amplitude change can be represented as a summation of different frequencies that change across time. Fourier transform can further analyze the frequency content at each timepoint. In addition, spectrograms can be further used to display both frequency and time domains. An additional axis of a power spectrogram represents the corresponding power of the frequency displayed. To accomplish that, first a custom-made script was generated to collect all stimulation-evoked responses. Spectrograms were made for each individual trial. Additionally, the signal due of stimulation was subtracted out of all trials.

Furthermore, we used the Chronux toolbox to generate spectrograms for each trial [76]. Specifically, in Chronux we employed a multi-taper spectrogram which is a spectral density estimation technique and is used to overcome bias and variance [77, 78].

Lastly the mean power of each trial and their corresponding pre-stimulation and post-stimulation was calculated. This was calculated for the frequency bands mentioned in Section 3.1 (theta, alpha, beta, and gamma). First the sampling frequency of 30 kHz was downsampled to 1 kHz. Next, a butterworth filter of order 4 was applied to the pre-stimulation and post-stimulation phase. The butterworth filter is a flat filter that allows for a high quality signal within the passband but has a drawback due to slow roll-off – hence a higher order filter is useful [69]. Here, we used Hilbert transform as it allows for an instantaneous phase to be calculated and is a powerful tool that gives out the analytical component while removing a ‘linear phase’ [69, 79]. Mann Whitney tests and Kruskal-Wallis tests were then completed in GraphPad Prism.

3.3 Results

3.3.1 Optimization of the Stimulation Protocol

In animals with unilateral implants and ground electrodes, an impedance of <100 kOhm was achieved without noisy raw signals. Additionally, in bilateral implants without ground electrodes, noise-filled data was recorded therefore these mice were not used in analysis.

Since I noticed a pronounced response at 30 μA, we went down to 15 μA as the maximum amplitude current. We also wished to ascertain whether 10 μA was also successful enough to induce neuroplasticity. Our ultimate goal is to achieve a therapeutic window that can help us attain a response with the lowest pulse width and the lowest amplitude current [73]. This is further described in Section 3.1.

3.3.2 A Comparison of Raw Amplitude-Time Plots of Heterozygous and Wildtype mice with 10 μA Amplitude Current

We first plotted raw electrophysiological recording to visualize neural activity prior to, during, and following the stimulation phase in all the trials. Many of these trials had an increased amplitude response from beforehand that indicates movement of mice while running.

Increased amplitude also resulted at times as a result of stimulation – when electrical stimulation was given behaviors such as tail movement, shutting of eyes, and rubbing of nose with paws were observed.

The amplitude trials noted in the figure below Figure 3.6 shows raw data recoded using 10 μA stimulation amplitude. The rest of the parameters such as frequency and pulse width remained the same (130 Hz, 100 μs).

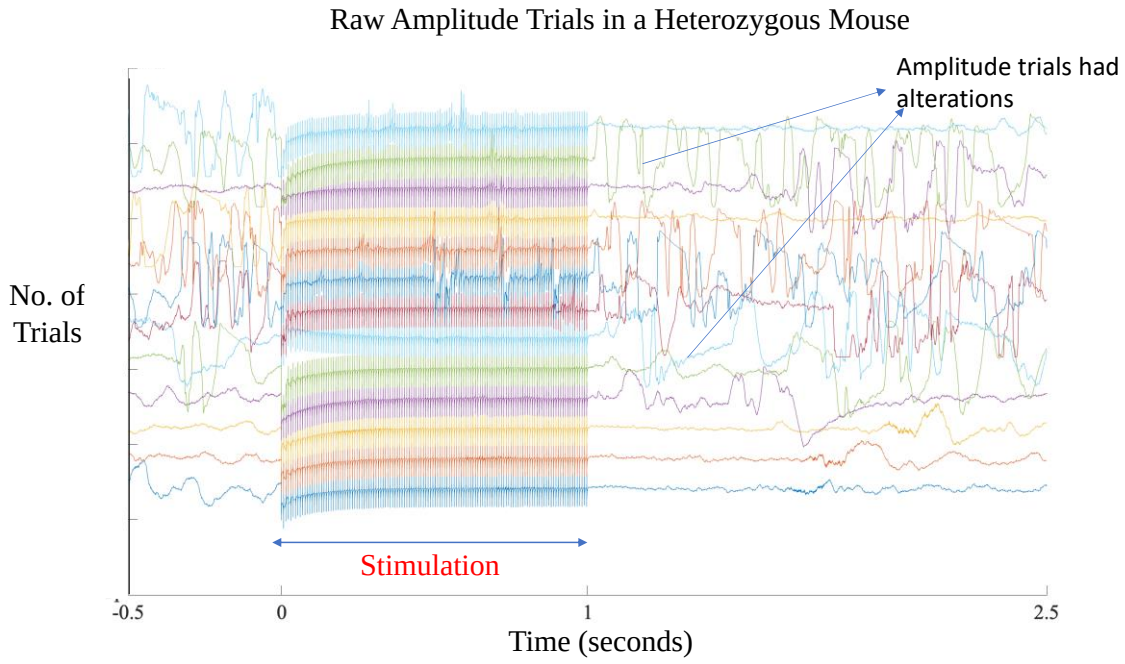

Figure 3.6: Raw trials are demonstrated on amplitude-time axis. The stimulation phase of 1 second is shown. Here, 130 pulses are given at each trial. Here, it was noted that the amplitude waveform in the heterozygous mouse was far more inconsistent when the pre-stimulation phase and post-stimulation phase was compared. The amplitudes shown here are off-set – this means each of the individual trials were within an amplitude range of 5000 μV but are displayed here as a representation.

Similar observations were noted in the wildtype mouse (Figure 3.7). As the electrophysiological recordings were completed in real-time, it was noticed increased movement such as running of the mouse or rubbing of nose using paws brought on a higher amplitude waveform. Upon analysis of raw signals, it was noticed that the wildtype mouse had more consistent amplitude trials. This meant a higher amplitude waveform in the wildtype mouse in the pre-stimulation phase resulted in a higher amplitude waveform in the post-stimulation phase.

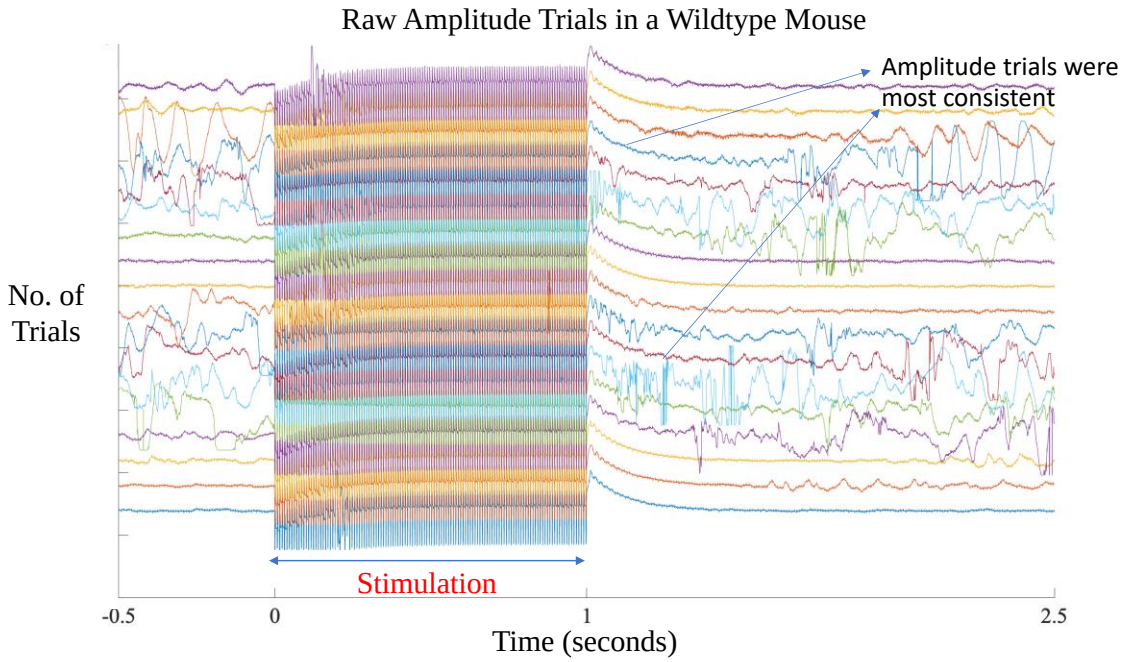

Figure 3.7: Raw trials are demonstrated on amplitude-time axis for the wildtype mouse and the stimulation phase of 1 second is shown. Again, 130 pulses are given at each trial. Here, it was noted that the amplitude waveform in the wildtype mouse was far more consistent when the pre-stimulation phase and post-stimulation phase was compared. Some post-trials had an increased amplitude, and they were also preceded by an increased amplitude in the pre-stimulation phase. The amplitudes shown here are again off-set as described in Figure 3.6.

In the set of trials of a wildtype mouse, it was noted that the impedance was at 143 kΩ, when ideally the impedance should be below 100 kΩ. To further analyze whether these amplitude changes with time had a difference between the disease state and control we assessed individual power spectrograms in the next section.

3.3.3 Individual Power Spectrograms of Heterozygous mice showed 50 dB power response from 7.32 to 51.3 Hz consistently in Individual Trials

To further characterize the local field potentials at the basolateral amygdala, we sought to implement a multitaper power spectrogram as described in Section 3.2.4. To obtain these spectrograms raw amplitude-time plots were plotted after which the stimulus-based amplitude was subtracted from each trial. After going over individual spectrogram trials, it was noticed a 50 dB response was present in the trials pertaining to heterozygous mice in the frequency range of 7.32 – 51.3 Hz as shown in Figure 3.8. The stimulation phase even though subtracted, still shows some

residual artifacts. Here we also noticed power between 20 – 40 dB frequency range of 51.3 – to 146 Hz.

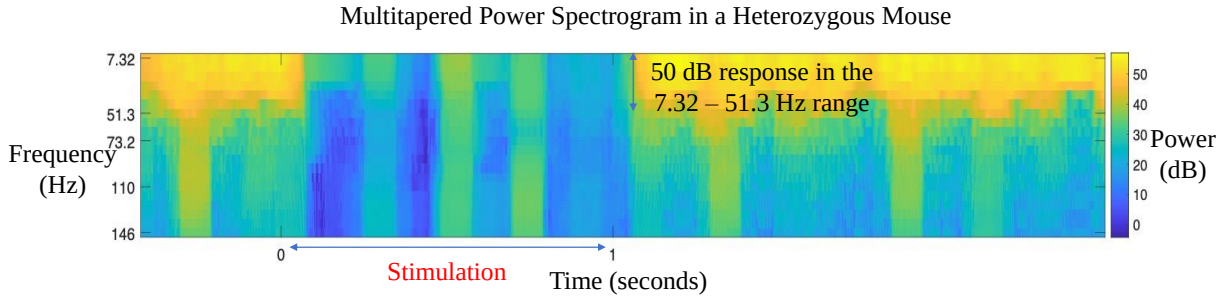

Figure 3.8: An individual trial is shown here with the pre-stimulation and post-stimulation phase represented. The stimulation phase lasted 1 second and is subtracted out there showing power from 0 – 20 dB, yet still artifacts can be visualized. The arrow in blue and in the post-stimulation phase points towards a 50 dB response in the 7.32 – 51.3 Hz range. Additionally, the pre-stimulation and post-stimulation phase also showed power in the 51.3 – 146 Hz range (20 – 30 dB)

Furthermore, we evaluated the individual power spectrograms in a wildtype mouse (Figure 3.9). In our wildtype mouse, stimulus artifacts were consistently noted in each of our trials for wildtype mice. We also did not notice a robust response to stimulation in the wildtype model compared to the heterozygous model.

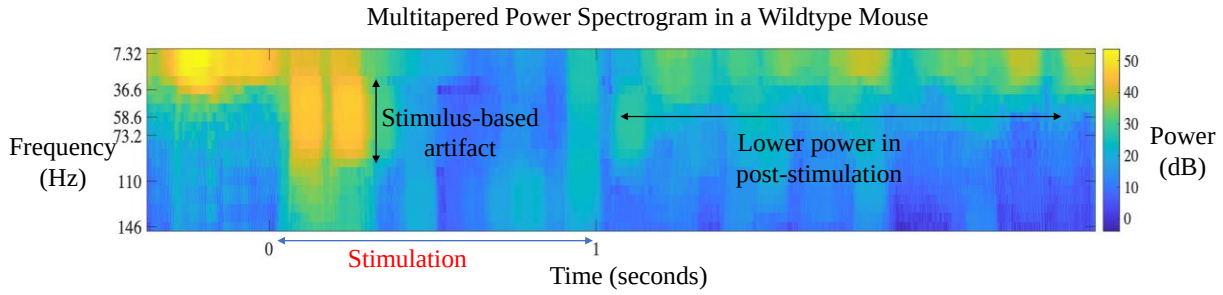

Figure 3.9: An individual trial is shown here with the pre-stimulation and post-stimulation phase represented. The stimulation phase lasted 1 second and is subtracted out there showing power from 0 – 50 dB, and here artifacts are clearly visualized. The post-stimulation phase points towards a 0 – 30 dB power. The 0 dB power range is present consistently between 36.6 – 146 Hz. Additionally, the pre-stimulation phase has a power response between 7.32 – 36.6 Hz (50 dB)

Additionally, it was noted in Figure 3.9 that if a 50 dB response was noted it was more concentrated in the 7.32 – 36.6 Hz range (in comparison to heterozygous mice where the 50 dB response had a higher frequency range of 51.3.

Viewing spectrograms allowed us to in assess the frequency content in time along with their respective power in dB. To further quantify the mean power, we additionally calculated the mean power in each respective frequency domain as described in Section 3.3.4 and 3.3.5.

3.3.4 Mean Power of Heterozygous and Wildtype Local Field Potentials in the Theta range

To perform further analysis on quantification of mean power of the theta range, we first extrapolated pre-stimulation phases of 0.5 seconds, and post-stimulation phases of 2.5 seconds for each individual spectrogram trial. As described in Section 3.1 our original interest is in theta and gamma as both these frequency waveforms correspond highly to BLA depending on the state of fear or safety. After attaining the pre-stimulus and post-stimulus phases, we then calculated the mean power with 95 % confidence interval (CI) of each trial using Hilbert transform. This was then averaged and is represented in Figure 3.10 for the theta wave in the range of 4 – 8 Hz (Figure 3.10).

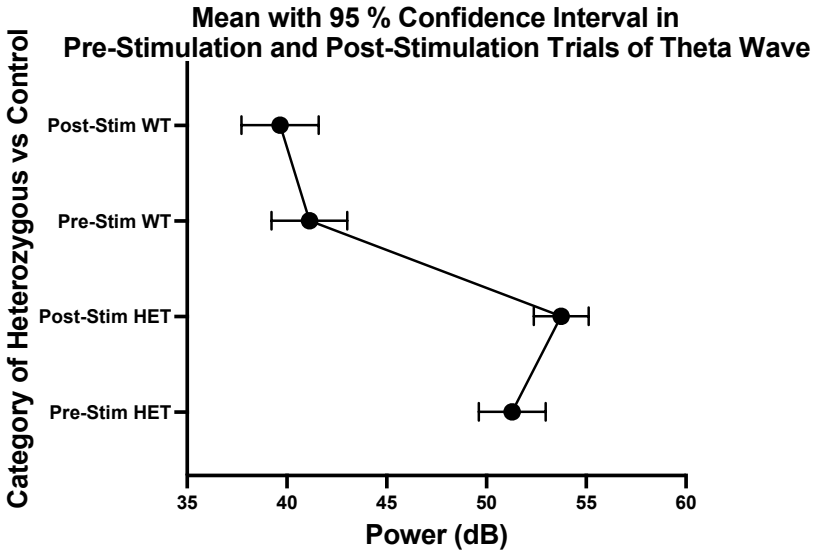

Figure 3.10: After collecting pre-stimulation and post-stimulation power responses for heterozygous (n = 89) and wildtype (n = 92), we plotted the data to represent the mean and 95 % CI. Kruskal-Wallis test was significant among all trials regardless of heterozygous or wildtype state. Specifically, the post-stimulation phase in the heterozygous model had a mean power of 53.7 dB (52.4 – 55.1 dB)

The wildtype mouse model had a lower power response in the theta range, regardless of the pre-stimulation (mean = 41.1 dB) or post-stimulation phase (mean = 39.7 dB). It was also noted that the wildtype model stimulation did not evoke a higher power response in the theta range.

This was in comparison to the heterozygous mice model where the pre-stimulation (mean = 51.3 dB) and post-stimulation (mean = 53.7 dB) power was higher. These differences were statistically significant through Kruskal Wallis test ($p < 0.0001$). Kruskal-Wallis test was performed instead of ANOVA due to the data not being normally distributed (Shapiro-Wilk test).

3.3.5 Mean Power in the Heterozygous and Wildtype Local Field Potentials mice in the Gamma Range

Here, we performed similar analysis as described in Section 3.3.4 to compute the average power across trials. Specifically, power was derived for the frequency range of 35 – 80 Hz (Figure 3.11). Similar patterns were observed between heterozygous and wildtype mice as detailed in Section 3.3.4. The heterozygous mouse model (n = 89) had the highest power response in the post-stimulation phase (mean = 41.4 dB; CI = 40.3 – 42.5 dB). As noted in the figure below, the pre-stimulation power response in the heterozygous model was 40.8 dB (CI = 39.5 – 42.1 dB).

Wildtype mice had a lower power response in the pre-stimulation phase (37.0 dB, CI = 35.5 – 38.5 dB) and post-stimulation phase (mean 36.8 dB; CI = 35.5 – 38.1 dB). It was noted the post-stimulation did not evoke a higher power response in the wildtype model compared to the heterozygous model – this observation is also described for theta waves in Section 3.3.4.

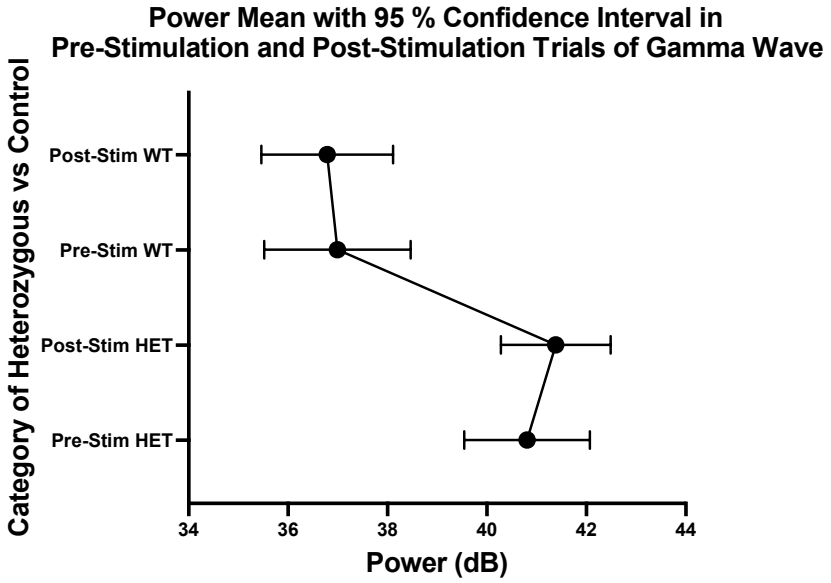

Figure 3.11: After collecting pre-stimulation and post-stimulation power responses for heterozygous (n = 89) and wildtype (n = 92) mice, we plotted the data to represent the mean and 95 % CI. Kruskal-Wallis test was significant among all trials regardless of heterozygous or wildtype state. Specifically, the post-stimulation phase in the heterozygous model had a mean power of 41.4 dB (40.3 – 42.5 dB)

Overall, it was found that the power in gamma range was much lesser compared to theta range when each of the means were compared. For instance, the heterozygous post-stimulation power in the theta range was 51.3 dB, and in the gamma range was 41.4 dB.

3.4 Conclusions

As noted in the previous literature described, we have noticed varied frequency responses post-stimulation that points more to the highly complex nature of BLA. For instance in a sample of 13 trials, 10 of the trials had a frequency response in the range of 7 – 51 Hz for the heterozygous model. Whether these differences exist due to memory changes (trials with theta wave) or due to state of safety (trials with gamma waves) can be even further assessed if local field potential recordings are collected while executing fear conditioning tests. Thus, future directions include combining fear conditioning tests with each stimulation trial will also be a useful strategy.

At present, our data showed power in the theta and gamma range changing particularly in the heterozygous model compared to the wildtype model. The theta power overall was also found to be greater compared to gamma power. These differences were also found to be significant between heterozygous and wildtype mice.

As detailed in the Introduction chapter, the extensive connections of BLA to other structures can provide us with useful data in the form of LFPs. These structures include the hippocampus, medial prefrontal cortex, and the motor cortex. Therefore, assessing the frequency content by placing recording electrodes at these sites will be another approach to explore the complex nature of BLA oscillations [51, 52, 70]. This is especially important as after the trials were completed the mice (both heterozygous and wildtype) seemed calm and were exhibiting less locomotor activity which could tie in with BLA's connections with the motor cortex [51]. Additionally, behavior analysis correlated with each stimulation trial will also be a useful strategy.

4. CONCLUSIONS AND FUTURE DIRECTIONS

Taken together, we have established a model of DBS translatable to other neurodevelopmental disorders. The first aim of such experiments is to develop a chronic surgical model where mice can survive, and DBS can be given. The scientific long-term goal for these experiments is to establish a model to assess synaptic plasticity on electrophysiological, behavioral, and proteomic scales, using the experimental methods generated in the study. The ultimate goal of these experiments is to generate preclinical data that can be translated to children, adolescents and adults suffering from ASD and co-occurring ID. The nature of this work is interdisciplinary including aspects of neural engineering, neuroscience, psychiatry, and neurosurgery – therefore, success in this project will benefit greatly from collaborative work at both preclinical and clinical stages.

4.1 DBS Surgical Protocol

4.1.1 Implications of DBS Surgery in Autism Models

The training phase comprised of at least n = 15 craniotomies and at least n = 22 headplate surgeries. This number does not include the surgeries that were done on wildtype mice for practice. Here, many of the results were removed from analysis, due to complications during surgery or anesthesia. As the experimenter commits to more surgeries the complications can be avoided to ensure recovery of mice. Complications in the training phase include unintentional removal of the headplate while attaching to the optical post assembly (Thor Labs) and refining the technique to ensure the vessels associated with the periosteum are avoided so bleeding at site of burr hole is minimal.

Apart from surgical complications, the mice had improved recovery once anesthetic complications were assessed and integrated into experiments. However, time and valuable resources were spent before realizing the stark differences between heterozygous and wildtype mice. Interestingly, my observations on variable responses to anesthesia discussed in section 2.3.2 above, mirror those observed anesthetic differences in another mouse model of ASD, the Shank3 haplotype truncation [65].

Of the training experiments I conducted (n = 15), in 3 mice I tested the significance and need of a ground electrode. Here, (Section 2.3.1), I tested whether two bilateral electrode implants at right and left basolateral amygdala without the ground electrode will result in neurophysiological readings. Importantly, these experiments were unsuccessful in that we did not receive electrophysiological recordings that were local field potentials, and instead attained only noise from both channels. From that, I concluded that implanting a ground electrode approximated close to the cortical surface was necessary.

At the end of our pilot phase of experiments, I was able to collect neurophysiological recordings that were indeed local field potentials from a total of three mice, of which two were heterozygous, i.e. the ASD model, and one was of wildtype genotype. A summary of the workflow of pilot experiments are shown in Figure 4.1.

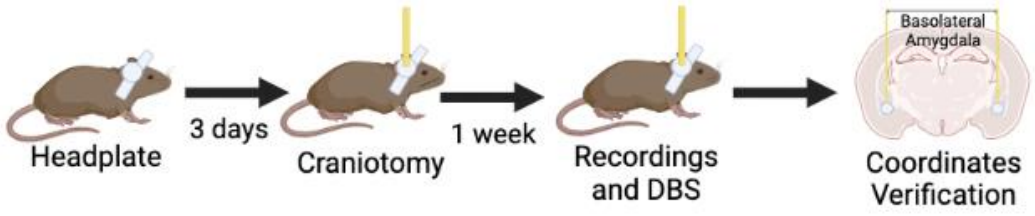

Figure 4.1: A summary of the workflow I employed in the pilot experiments. The mouse (3 – 4 months) would first undergo headplate surgery, followed by craniotomy and electrode placement after 3 days of recovery. Approximately 1 – 2 weeks post-surgery, the mouse was stimulated and local field potentials were recorded. At the end of the study, the insertion site was lesioned and verified with histology.

4.1.2 Future Directions of DBS Surgery in Autism Mice Models

Since mice are a much smaller model in comparison to rats and monkeys, there can be a considerable error in pinpointing the correct nucleus to stimulate. Previous studies have used histological verification to identify the correct nucleus [30, 55, 64]. Other methods include having an electrophysiological apparatus right in close proximity to the surgical suite – hence as the electrode is being descended, the correct nucleus can be determined. Therefore, oscillations can be determined during the surgery [80]. Lastly, a few studies have also combined the DBS surgery with magnetic resonance imaging (MRI) recordings [81]. Together, these approaches will need extensive resources and setup. The alternative experiments detailed here have a notable learning curve – though once the optimization is done, more robust and accurate data can be collected.

For our preliminary studies, we chose BLA as a target based on clinical case studies and its relevance for ASD. However, future studies must define the role of other targets in DBS surgery such as nucleus accumbens and globus pallidus [9, 25]. The questions that remain unanswered is at the preclinical level – how can we better choose targets based on the genetics and symptoms of the patient with autism? Furthermore, during the translational phase to humans the next question to address will be based on the symptomatology and functional MRI imaging studies conducted in the patients. This poses the question on how can personalized targets to the brain be decided? It must be noted however, that collating such data for translational studies in humans is based on rigorous studies at the preclinical level.

4.2 Electrophysiology

4.2.1 Implications of Stimulation based Electrophysiology in *Syngap1*$^{+/-}$ mice

Previous literature has identified the presence of delta, theta, and gamma oscillations in the BLA region and the oscillations vary widely based on the state the rodent exists in [70]. Therefore, in our study we did see theta oscillations with greater power as shown in our spectrograms (Figure 3.8). Of note, however, during stimulation trials, increased running of the mice was associated with greater amplitude (Figure 3.6 and Figure 3.7). Therefore, there is a need during analysis to extract trials associated with higher amplitude because of running and analyzing them separately. Heightened motor responses in response to stimulation in both heterozygous and wildtype mice could be explained by the extensive projections to motor cortex and sensory cortex from BLA [82]. This is described in further detail in Section 3.4. As noted in Chapter 3, our data did find a robust power response in post-stimulation theta and gamma in the heterozygous model. This data could be further correlated with fear conditioning tests as it relates to *Syngap1*$^{+/-}$ mice as described in Section 3.4 [70].

4.2.2 Future Directions of Electrical Stimulation in *Syngap1*$^{+/-}$ mice

Throughout the stimulation trials, I noticed different behaviors of awake, freely moving mice (Section 3.4). The behavior was noted consistently throughout trials, but this data is not shown as a formal experiment on correlating behavior with electrophysiology was not conducted.

Additionally, in the heterozygous mice model, I also noticed the mice were very calm and were not exhibiting aggressive movements (data not shown). To understand these processes, it will be beneficial to conduct behavior analysis integrated with local field potentials recordings. This will help us in correlating each of the stimulation trials and their corresponding frequency content with the respective behavior noted in the mouse.

Anatomically, there are also different fibers consisting of glutamatergic fibers and GABAergic fibers projecting within the BLA [83, 84]. To understand which type of fiber is implicated in pathogenesis, future studies may also include using optogenetics based stimulation to precisely target the fibers [55].

4.3 Behavior

4.3.1 Implications of Behavioral Assessment in *Syngap1*$^{+/-}$ mice

Extensive studies have assessed behavior in *Syngap1*$^{+/-}$ mice, with impairments in social, memory and fear conditioning in *Syngap1*$^{+/-}$ haploinsufficient mice compared to neurotypical wildtype littermates [29, 85]. Building from the workflow of experimentation we have developed in our pilot study, our ongoing experiments include conducting behavioral tests in these mice to study the efficacy of DBS. The behavioral tests we are going to employ to date include open field tests, Crawley's sociability and novel object recognition test (Figure 4.3) [29, 85, 86].

Previous literature has shown increased locomotor activity, as assessed by monitoring movement within an open field chamber. The increased locomotor activity was present in heterozygous mice in comparison to wildtype mice during open field tests. This is further explained by their hyperactivity [85].

Crawley's sociability is a standardized test for autism mouse models that quantifies the innate response of a rodent to interact with stranger mice [87]. Previous studies showed that the *Syngap1*$^{+/-}$ heterozygous mice spend less time around stranger mice in comparison with wildtype mice [85]. This was also shown in my preliminary experiments for heterozygous ($n = 5$) and wildtype ($n = 5$) (Figure 4.2). Although a trend was noticed of heterozygous mice spending less time around stranger mice, at present my results were not statistically significant using unpaired t test ($p = 0.731$). This may be explained by the small cohort, that was also composed of a mixture of ages and sexes. Therefore, increasing these numbers and separating out these variables may

strengthen these data. In our ongoing experiments we found it was essential to handle mice following recovery – therefore our current workflow for Crawley's sociability includes at least 2 handling days, a habituation day and finally the testing day.

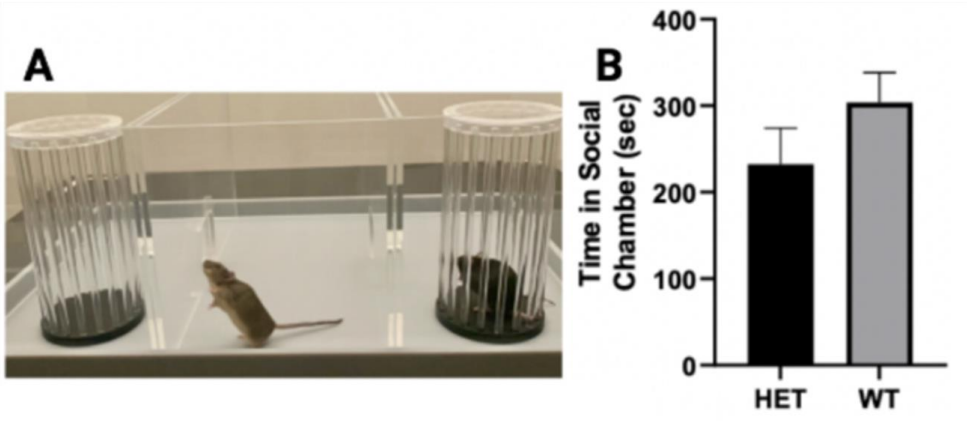

Figure 4.2: Crawley's sociability in *Syngap1*$^{+/-}$ mice. A) Test mice are kept in a three- chamber apparatus while stranger mice are enclosed. B) Heterozygous mice spent less time around stranger mouse, however these results were not statistically significant.

Additionally, novel object recognition test is another test that is now widely adopted. The basis of the test explores the rodent's innate ability to explore new objects, where the discrimination index is ascertained. The test ultimately assesses cognition, learning and memory. The most research has shown reversal of deficits in discrimination index when a GSK-3β inhibitor, 6-bromoindirubin-3`-oxime (6BIO) was used to improve synaptic transmission in *Syngap1*$^{+/-}$ mice [47].

Our current workflow of experiments is described below (Figure 4.3). Here, we aim to conduct DBS stimulation on the testing day in both novel object recognition tests, and Crawley's sociability. My hypothesis is that DBS prior to behavioral assessment will reduce hyperactivity (open field), improve social interaction (Crawley's sociability), and increase freezing (contextual and cued fear conditioning) and improve memory (object recognition) in the *Syngap1*$^{+/-}$ mice at comparable levels to wildtype. There are several reasons for this hypothesis. Previously, behavioral tests of fear conditioning have improved in *Syngap1*$^{+/-}$ mice following re-expression of SynGAP protein [46]. As stated in the Introduction chapter, previous preclinical literature has demonstrated improvement in behavioral tests in ASD mouse models [26, 28].

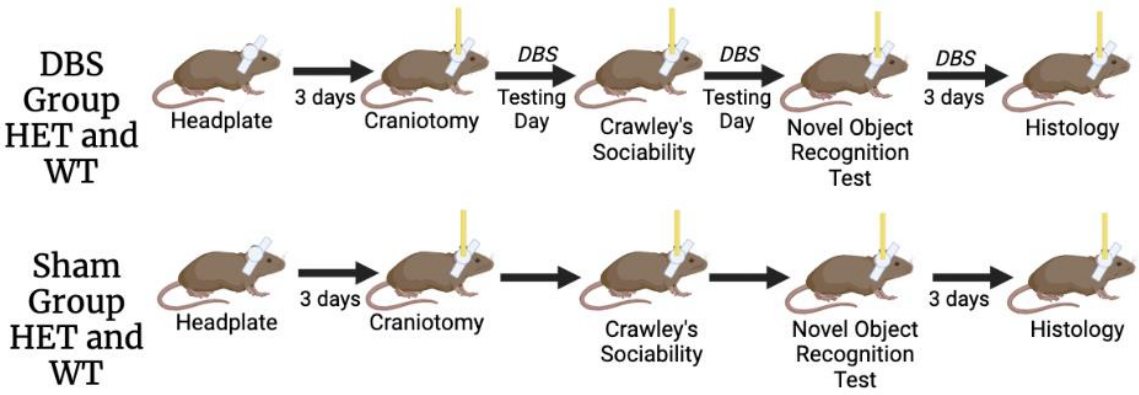

Figure 4.3: A workflow of ongoing experiments demonstrating behavioral experimentation in DBS (active electrode) and sham (electrode not used for stimulation) mice. Sham mice undergo the same surgery but without stimulation. Once the surgeries are completed, mice should be given a 1-week recovery phase before testing commences. DBS can then be given on testing days of Crawley's sociability and novel object recognition test. At least 3 days gap should be given between Crawley's sociability and novel object recognition test.

4.3.2 Future Directions of Behavioral Assessment in *Syngap1*$^{+/-}$ mice

Future directions of behavioral analysis include conducting fear conditioning tests. Here, it will be integral to ascertain the theta oscillations that are present in the state of threat (with conditioned stimulus) and fast gamma oscillations present in the state of safety (without conditioned stimulus) [46, 70]. Similar to our current experiments trials of stimulations can be given on the testing day and LFPs recorded after the last day of experimentation that involves contextual fear conditioning [88]. Additionally, mice receiving DBS can be compared with sham control mice to see if differences in these oscillations exist.

4.4 Synaptic Plasticity in the Context of Proteomic Correlates

4.4.1 Preliminary and Future Experiments to assess labeling in adult mice

DBS as a therapeutic ailment can induce neuroplasticity. This was demonstrated in a study that showed forniceal DBS used in Rett syndrome mouse model resulted in upregulated genes associated with synaptic plasticity [30, 64]. We therefore deduce that DBS at BLA regulates protein synthesis to generate newly synthesized proteins (NSPs) throughout the brain, particularly at the hippocampus where molecular changes associated with SynGAP1 protein occur [29, 89].

Prior proteomic analyses of the post-synaptic density (PSD) in ASD models have revealed prime differences in the hippocampus and striatum indicating the hippocampal tissue as a target of interest in our analysis [64, 90]. Moreover, recent studies have shown DBS can also induce short-term plasticity [90]. Therefore, future directions include studying proteomic changes via BioOrthogonal Non-Canonical Amino Acid Tagging (BONCAT) followed by tandem Mass Spectrometry (LC-MS/MS) analysis to identify specific proteins along with fluorescence non-canonical amino acid tagging (FUNCAT) to visualize and spatially analyze the protein alterations. BONCAT allows tracking of newly synthesized proteins through non-canonical amino acids (NCAA) such as L-azidohomoalanine (AHA).

Furthermore, we are currently optimizing protein labeling strategies [91] in combination with fluorescent non-canonical amino acid tagging (FUNCAT) [92].

In our preliminary data broad labeling was noticed in adult mice samples. This meant labeling was seen however the signal attained over background was lower in P77 mice compared to P16 mice. Thus, the primary goals will be to use BONCAT followed by LC-MS/MS on hippocampal tissue collected from sham and DBS mice to study differences in plasticity. This will tie in with the previously introduced concept of elevated basal protein synthesis in heterozygous mice and whether that gets alleviated with DBS. This will also aid us in identifying any newly synthesized proteins that are present in response to stimulation.

4.5 Final Thoughts on Long-Term Goals

To conclude, I have demonstrated through this project presence of sustained theta oscillations (Figure 3.10) with increased power following DBS in a mouse model of ASD. As demonstrated in this chapter, there are many unanswered questions on how DBS will cause synaptic plasticity on electrophysiological, behavioral, and proteomic scales. Of note, there is great potential to address unanswered questions regarding how regulatory functions of synaptic proteins can be restored following DBS. Furthermore, future directions will include validating this model across other models of autism to ensure any future potential in translating this research to the clinic.

REFERENCES

[1] E. T. Newcomb and L. P. Hagopian, "Treatment of severe problem behaviour in children with autism spectrum disorder and intellectual disabilities," *Int. Rev. Psychiatry Abingdon Engl.*, vol. 30, no. 1, pp. 96–109, Feb. 2018, doi: 10.1080/09540261.2018.1435513.

[2] S. S. Jeste and D. H. Geschwind, "Disentangling the heterogeneity of autism spectrum disorder through genetic findings," *Nat. Rev. Neurol.*, vol. 10, no. 2, pp. 74–81, Feb. 2014, doi: 10.1038/nrneurol.2013.278.

[3] M. Junaid *et al.*, "Association between craniofacial anomalies, intellectual disability and autism spectrum disorder: Western Australian population-based study," *Pediatr. Res.*, pp. 1–10, Mar. 2022, doi: 10.1038/s41390-022-02024-9.

[4] D. M. James, E. A. Davidson, J. Yanes, B. Moshiree, and J. E. Dallman, "The Gut-Brain-Microbiome Axis and Its Link to Autism: Emerging Insights and the Potential of Zebrafish Models," *Front. Cell Dev. Biol.*, vol. 9, p. 662916, Apr. 2021, doi: 10.3389/fcell.2021.662916.

[5] S. E. Fitzpatrick, L. Srivorakiat, L. K. Wink, E. V. Pedapati, and C. A. Erickson, "Aggression in autism spectrum disorder: Presentation and treatment options," *Neuropsychiatr. Dis. Treat.*, vol. 12, 2016.

[6] E. Patten, K. K. Ausderau, L. R. Watson, and G. T. Baranek, "Sensory Response Patterns in Nonverbal Children with ASD," *Autism Res. Treat.*, vol. 2013, p. e436286, Jul. 2013, doi: 10.1155/2013/436286.

[7] A. Thurm, C. Farmer, E. Salzman, C. Lord, and S. Bishop, "State of the Field: Differentiating Intellectual Disability From Autism Spectrum Disorder," *Front. Psychiatry*, vol. 10, p. 526, Jul. 2019, doi: 10.3389/fpsyt.2019.00526.

[8] F. F. Hamdan *et al.*, "De novo mutations in FOXP1 in cases with intellectual disability, autism, and language impairment," *Am. J. Hum. Genet.*, vol. 87, no. 5, pp. 671–678, Nov. 2010, doi: 10.1016/j.ajhg.2010.09.017.

[9] H. R. Park *et al.*, "Nucleus accumbens deep brain stimulation for a patient with self-injurious behavior and autism spectrum disorder: functional and structural changes of the brain: report of a case and review of literature," *Acta Neurochir. (Wien)*, vol. 159, no. 1, pp. 137–143, Jan. 2017, doi: 10.1007/s00701-016-3002-2.

[10] S. Sinha, R. A. McGovern, and S. A. Sheth, "Deep brain stimulation for severe autism: from pathophysiology to procedure," *Neurosurg. Focus*, vol. 38, no. 6, p. E3, Jun. 2015, doi: 10.3171/2015.3.FOCUS1548.

[11] E. Courchesne, "Brain development in autism: early overgrowth followed by premature arrest of growth," *Ment. Retard. Dev. Disabil. Res. Rev.*, vol. 10, no. 2, pp. 106–111, 2004, doi: 10.1002/mrdd.20020.

[12] C. Bagni and R. S. Zukin, “A Synaptic Perspective of Fragile X Syndrome and Autism Spectrum Disorders,” *Neuron*, vol. 101, no. 6, pp. 1070–1088, Mar. 2019, doi: 10.1016/j.neuron.2019.02.041.

[13] V. Verma, A. Paul, A. Amrapali Vishwanath, B. Vaidya, and J. P. Clement, “Understanding intellectual disability and autism spectrum disorders from common mouse models: synapses to behaviour,” *Open Biol.*, vol. 9, no. 6, p. 180265, doi: 10.1098/rsob.180265.

[14] S. LeClerc and D. Easley, “Pharmacological Therapies for Autism Spectrum Disorder: A Review,” *Pharm. Ther.*, vol. 40, no. 6, pp. 389–397, Jun. 2015.

[15] D. Granpeesheh, J. Tarbox, and D. Dixon, “Applied behavior analytic interventions for children with autism: A description and review of treatment research,” *Ann. Clin. Psychiatry Off. J. Am. Acad. Clin. Psychiatr.*, vol. 21, pp. 162–73, Aug. 2009.

[16] L. Pycroft, J. Stein, and T. Aziz, “Deep brain stimulation: An overview of history, methods, and future developments,” *Brain Neurosci. Adv.*, vol. 2, p. 2398212818816017, Jan. 2018, doi: 10.1177/2398212818816017.

[17] J. M. Schwalb and C. Hamani, “The history and future of deep brain stimulation,” *Neurother. J. Am. Soc. Exp. Neurother.*, vol. 5, no. 1, pp. 3–13, Jan. 2008, doi: 10.1016/j.nurt.2007.11.003.

[18] M. S. Okun, J. Green, R. Saben, R. Gross, K. D. Foote, and J. L. Vitek, “Mood changes with deep brain stimulation of STN and GPi: results of a pilot study,” *J. Neurol. Neurosurg. Psychiatry*, vol. 74, no. 11, pp. 1584–1586, Nov. 2003, doi: 10.1136/jnnp.74.11.1584.

[19] C. R. P. Sullivan, S. Olsen, and A. S. Widge, “Deep brain stimulation for psychiatric disorders: From focal brain targets to cognitive networks,” *NeuroImage*, vol. 225, p. 117515, Jan. 2021, doi: 10.1016/j.neuroimage.2020.117515.

[20] J. J. Langille and R. E. Brown, “The Synaptic Theory of Memory: A Historical Survey and Reconciliation of Recent Opposition,” *Front. Syst. Neurosci.*, vol. 12, p. 52, Oct. 2018, doi: 10.3389/fnsys.2018.00052.

[21] C. C. McIntyre and R. W. Anderson, “Deep Brain Stimulation Mechanisms: The Control of Network Activity via Neurochemistry Modulation,” *J. Neurochem.*, vol. 139, no. Suppl 1, pp. 338–345, Oct. 2016, doi: 10.1111/jnc.13649.

[22] P. Mateos-Aparicio and A. Rodríguez-Moreno, “The Impact of Studying Brain Plasticity,” *Front. Cell. Neurosci.*, vol. 13, 2019, Accessed: Dec. 05, 2022. [Online]. Available: https://www.frontiersin.org/articles/10.3389/fncel.2019.00066

[23] H. Yan *et al.*, “An open-label prospective pilot trial of nucleus accumbens deep brain stimulation for children with autism spectrum disorder and severe, refractory self-injurious behavior: study protocol,” *Pilot Feasibility Stud.*, vol. 8, no. 1, p. 24, Feb. 2022, doi: 10.1186/s40814-022-00988-3.

[24] V. Sturm *et al.*, “DBS in the basolateral amygdala improves symptoms of autism and related self-injurious behavior: a case report and hypothesis on the pathogenesis of the disorder,” *Front. Hum. Neurosci.*, vol. 6, p. 341, 2012, doi: 10.3389/fnhum.2012.00341.

[25] A. Stocco and J. F. Baizabal-Carvallo, “Deep brain stimulation for severe secondary stereotypies,” *Parkinsonism Relat. Disord.*, vol. 20, no. 9, pp. 1035–1036, Sep. 2014, doi: 10.1016/j.parkreldis.2014.06.019.

[26] T.-C. Lin *et al.*, “MR imaging central thalamic deep brain stimulation restored autistic-like social deficits in the rat,” *Brain Stimulat.*, vol. 12, no. 6, pp. 1410–1420, Dec. 2019, doi: 10.1016/j.brs.2019.07.004.

[27] H.-F. Wu *et al.*, “Deep Brain Stimulation Modified Autism-Like Deficits via the Serotonin System in a Valproic Acid-Induced Rat Model,” *Int. J. Mol. Sci.*, vol. 19, no. 9, p. 2840, Sep. 2018, doi: 10.3390/ijms19092840.

[28] A. D. Chang, V. A. Berges, S. J. Chung, G. Y. Fridman, J. M. Baraban, and I. M. Reti, “High-Frequency Stimulation at the Subthalamic Nucleus Suppresses Excessive Self-Grooming in Autism-Like Mouse Models,” *Neuropsychopharmacology*, vol. 41, no. 7, pp. 1813–1821, Jun. 2016, doi: 10.1038/npp.2015.350.

[29] M. Muhia *et al.*, “Molecular and behavioral changes associated with adult hippocampus-specific SynGAP1 knockout,” *Learn. Mem.*, vol. 19, no. 7, pp. 268–281, Jul. 2012, doi: 10.1101/lm.026351.112.

[30] S. Hao *et al.*, “Forniceal deep brain stimulation rescues hippocampal memory in Rett syndrome mice,” *Nature*, vol. 526, no. 7573, pp. 430–434, Oct. 2015, doi: 10.1038/nature15694.

[31] L. Mapelli, T. Soda, E. D’Angelo, and F. Prestori, “The Cerebellar Involvement in Autism Spectrum Disorders: From the Social Brain to Mouse Models,” *Int. J. Mol. Sci.*, vol. 23, no. 7, p. 3894, Mar. 2022, doi: 10.3390/ijms23073894.

[32] P. G. Enticott *et al.*, “A double-blind, randomized trial of deep repetitive transcranial magnetic stimulation (rTMS) for autism spectrum disorder,” *Brain Stimulat.*, vol. 7, no. 2, pp. 206–211, Apr. 2014, doi: 10.1016/j.brs.2013.10.004.

[33] A. van Hoorn, T. Carpenter, K. Oak, R. Laugharne, H. Ring, and R. Shankar, “Neuromodulation of autism spectrum disorders using vagal nerve stimulation,” *J. Clin. Neurosci.*, vol. 63, pp. 8–12, May 2019, doi: 10.1016/j.jocn.2019.01.042.

[34] J. K. Luiselli, F. Bird, and L. E. Wachtel, “Electroconvulsive Therapy (ECT) for Autism Spectrum Disorder Associated with Catatonia and Self-Injury: a Clinical Review,” *Adv. Neurodev. Disord.*, vol. 5, no. 2, pp. 117–125, Jun. 2021, doi: 10.1007/s41252-021-00202-0.

[35] A. Wagle Shukla, P. Zeilman, H. Fernandez, J. A. Bajwa, and R. Mehanna, “DBS Programming: An Evolving Approach for Patients with Parkinson’s Disease,” *Park. Dis.*, vol. 2017, p. 8492619, 2017, doi: 10.1155/2017/8492619.

[36] O. DURMAZ, M. A. ATEŞ, and M. G. ŞENOL, “Repetitive Transcranial Magnetic Stimulation (rTMS)-Induced Trigeminal Autonomic Cephalalgia,” *Nöro Psikiyatri Arş.*, vol. 52, no. 3, pp. 309–311, Sep. 2015, doi: 10.5152/npa.2015.7618.

[37] T. R. Gamache, Y. Araki, and R. L. Huganir, “Twenty Years of SynGAP Research: From Synapses to Cognition,” *J. Neurosci.*, vol. 40, no. 8, pp. 1596–1605, Feb. 2020, doi: 10.1523/JNEUROSCI.0420-19.2020.

[38] Y. Araki *et al.*, “SynGAP isoforms differentially regulate synaptic plasticity and dendritic development,” *eLife*, vol. 9, p. e56273, Jun. 2020, doi: 10.7554/eLife.56273.

[39] E. Lee, J. Lee, and E. Kim, “Excitation/Inhibition Imbalance in Animal Models of Autism Spectrum Disorders,” *Biol. Psychiatry*, vol. 81, no. 10, pp. 838–847, May 2017, doi: 10.1016/j.biopsych.2016.05.011.

[40] J. P. Clement *et al.*, “Pathogenic SYNGAP1 Mutations Impair Cognitive Development by Disrupting Maturation of Dendritic Spine Synapses,” *Cell*, vol. 151, no. 4, pp. 709–723, Nov. 2012, doi: 10.1016/j.cell.2012.08.045.

[41] S. A. Barnes *et al.*, “Convergence of Hippocampal Pathophysiology in Syngap+/− and Fmr1−/y Mice,” *J. Neurosci.*, vol. 35, no. 45, pp. 15073–15081, Nov. 2015, doi: 10.1523/JNEUROSCI.1087-15.2015.

[42] S. M. Till *et al.*, “Conserved hippocampal cellular pathophysiology but distinct behavioural deficits in a new rat model of FXS,” *Hum. Mol. Genet.*, vol. 24, no. 21, pp. 5977–5984, Nov. 2015, doi: 10.1093/hmg/ddv299.

[43] W. C. Abraham, “Metaplasticity: tuning synapses and networks for plasticity,” *Nat. Rev. Neurosci.*, vol. 9, no. 5, Art. no. 5, May 2008, doi: 10.1038/nrn2356.

[44] H. Amal *et al.*, “Shank3 mutation in a mouse model of autism leads to changes in the S-nitroso-proteome and affects key proteins involved in vesicle release and synaptic function,” *Mol. Psychiatry*, vol. 25, no. 8, Art. no. 8, Aug. 2020, doi: 10.1038/s41380-018-0113-6.

[45] A. K. H. Toft, “Impact of two autism related genes on amygdala physiology,” Nov. 2019, Accessed: Jan. 29, 2022. [Online]. Available: https://era.ed.ac.uk/handle/1842/36625

[46] T. K. Creson *et al.*, “Re-expression of SynGAP Protein in Adulthood Improves Translatable Measures of Brain Function and Behavior in a Model of Neurodevelopmental Disorders,” Neuroscience, preprint, Nov. 2018. doi: 10.1101/474965.

[47] V. Verma *et al.*, “Reversing GABA polarity corrects synaptic physiology and behavioural deficits in young adolescent Syngap1+/- mice,” In Review, preprint, Jul. 2021. doi: 10.21203/rs.3.rs-682039/v1.

[48] D. Seguin, S. Pac, J. Wang, R. Nicolson, J. Martinez-Trujillo, and E. G. Duerden, "Amygdala subnuclei development in adolescents with autism spectrum disorder: Association with social communication and repetitive behaviors," *Brain Behav.*, vol. 11, no. 8, p. e2299, Aug. 2021, doi: 10.1002/brb3.2299.

[49] M. Fastenrath *et al.*, "Dynamic Modulation of Amygdala–Hippocampal Connectivity by Emotional Arousal," *J. Neurosci.*, vol. 34, no. 42, pp. 13935–13947, Oct. 2014, doi: 10.1523/JNEUROSCI.0786-14.2014.

[50] C. M. Schumann, C. Carter Barnes, C. Lord, and E. Courchesne, "Amygdala Enlargement in Toddlers with Autism Related to Severity of Social and Communication Impairments," *Biol. Psychiatry*, vol. 66, no. 10, pp. 942–949, Nov. 2009, doi: 10.1016/j.biopsych.2009.07.007.

[51] H. Hintiryan *et al.*, "Connectivity characterization of the mouse basolateral amygdalar complex," *Nat. Commun.*, vol. 12, no. 1, Art. no. 1, May 2021, doi: 10.1038/s41467-021-22915-5.

[52] A. Thompson *et al.*, "Impaired Communication Between the Motor and Somatosensory Homunculus Is Associated With Poor Manual Dexterity in Autism Spectrum Disorder," *Biol. Psychiatry*, vol. 81, no. 3, pp. 211–219, Feb. 2017, doi: 10.1016/j.biopsych.2016.06.020.

[53] G. Fernandes *et al.*, "Correction of amygdalar dysfunction in a rat model of fragile X syndrome," *Cell Rep.*, vol. 37, no. 2, p. 109805, Oct. 2021, doi: 10.1016/j.celrep.2021.109805.

[54] N. A. Herweg, E. A. Solomon, and M. J. Kahana, "Theta Oscillations in Human Memory," *Trends Cogn. Sci.*, vol. 24, no. 3, pp. 208–227, Mar. 2020, doi: 10.1016/j.tics.2019.12.006.

[55] N. S. Ahlgrim and J. R. Manns, "Optogenetic Stimulation of the Basolateral Amygdala Increased Theta-Modulated Gamma Oscillations in the Hippocampus," *Front. Behav. Neurosci.*, vol. 13, 2019, Accessed: Jan. 27, 2022. [Online]. Available: https://www.frontiersin.org/article/10.3389/fnbeh.2019.00087

[56] S. L. Hoogstraten-Miller and P. A. Brown, "TECHNIQUES IN ASEPTIC RODENT SURGERY," *Curr. Protoc. Immunol. Ed. John E Coligan Al*, vol. CHAPTER, p. Unit-1.12-14, Aug. 2008, doi: 10.1002/0471142735.im0112s82.

[57] M. Fleischer, H. Endres, M. Sendtner, and J. Volkmann, "Development of a Fully Implantable Stimulator for Deep Brain Stimulation in Mice," *Front. Neurosci.*, vol. 14, 2020, Accessed: Nov. 18, 2022. [Online]. Available: https://www.frontiersin.org/articles/10.3389/fnins.2020.00726

[58] M. E. Lopez, "A Quick, No Frills Approach to Mouse Genotyping," *Bio-Protoc.*, vol. 2, no. 15, p. e244, Aug. 2012.

[59] S. Jacquot, N. Chartoire, F. Piguet, Y. Hérault, and G. Pavlovic, "Optimizing PCR for Mouse Genotyping: Recommendations for Reliable, Rapid, Cost Effective, Robust and Adaptable to High-Throughput Genotyping Protocol for Any Type of Mutation," *Curr. Protoc. Mouse Biol.*, vol. 9, no. 4, p. e65, 2019, doi: 10.1002/cpmo.65.

[60] M. S. Hoseini, B. Rakela, Q. Flores-Ramirez, A. R. Hasenstaub, A. Alvarez-Buylla, and M. P. Stryker, “Transplanted Cells Are Essential for the Induction But Not the Expression of Cortical Plasticity,” *J. Neurosci.*, vol. 39, no. 38, pp. 7529–7538, Sep. 2019, doi: 10.1523/JNEUROSCI.1430-19.2019.

[61] “Neuroscience solutions - Microprobes for Life Science - Microprobes for Life Science.” https://microprobes.com/ (accessed Dec. 06, 2022).

[62] G. Deli *et al.*, “Comparison of the efficacy of unipolar and bipolar electrode configuration during subthalamic deep brain stimulation,” *Parkinsonism Relat. Disord.*, vol. 17, no. 1, pp. 50–54, Jan. 2011, doi: 10.1016/j.parkreldis.2010.10.012.

[63] E. Patrick, M. E. Orazem, J. C. Sanchez, and T. Nishida, “Corrosion of tungsten microelectrodes used in neural recording applications,” *J. Neurosci. Methods*, vol. 198, no. 2, pp. 158–171, Jun. 2011, doi: 10.1016/j.jneumeth.2011.03.012.

[64] A. E. Pohodich *et al.*, “Forniceal deep brain stimulation induces gene expression and splicing changes that promote neurogenesis and plasticity,” *eLife*, vol. 7, p. e34031, Mar. 2018, doi: 10.7554/eLife.34031.

[65] C. Li *et al.*, “Sensitivity to isoflurane anesthesia increases in autism spectrum disorder Shank3+/Δc mutant mouse model,” *Neurotoxicol. Teratol.*, vol. 60, pp. 69–74, Apr. 2017, doi: 10.1016/j.ntt.2016.11.002.

[66] Y. Yang and J.-Z. Wang, “From Structure to Behavior in Basolateral Amygdala-Hippocampus Circuits,” *Front. Neural Circuits*, vol. 11, 2017, Accessed: Dec. 04, 2022. [Online]. Available: https://www.frontiersin.org/articles/10.3389/fncir.2017.00086

[67] A. J. McDonald, “Functional neuroanatomy of the basolateral amygdala: Neurons, neurotransmitters, and circuits,” *Handb. Behav. Neurosci.*, vol. 26, pp. 1–38, 2020, doi: 10.1016/b978-0-12-815134-1.00001-5.

[68] G. Buzsáki, C. A. Anastassiou, and C. Koch, “The origin of extracellular fields and currents — EEG, ECoG, LFP and spikes,” *Nat. Rev. Neurosci.*, vol. 13, no. 6, Art. no. 6, Jun. 2012, doi: 10.1038/nrn3241.

[69] N. Maling and C. McIntyre, “Chapter 5 - Local Field Potential Analysis for Closed-Loop Neuromodulation,” in *Closed Loop Neuroscience*, A. El Hady, Ed. San Diego: Academic Press, 2016, pp. 67–80. doi: 10.1016/B978-0-12-802452-2.00005-6.

[70] M. Bocchio, S. Nabavi, and M. Capogna, “Synaptic Plasticity, Engrams, and Network Oscillations in Amygdala Circuits for Storage and Retrieval of Emotional Memories,” *Neuron*, vol. 94, no. 4, pp. 731–743, May 2017, doi: 10.1016/j.neuron.2017.03.022.

[71] J. M. Stujenske, E. Likhtik, M. A. Topiwala, and J. A. Gordon, “Fear and Safety Engage Competing Patterns of Theta-Gamma Coupling in the Basolateral Amygdala,” *Neuron*, vol. 83, no. 4, pp. 919–933, Aug. 2014, doi: 10.1016/j.neuron.2014.07.026.

[72] S. J. Groiss, L. Wojtecki, M. Südmeyer, and A. Schnitzler, “Deep Brain Stimulation in Parkinson’s Disease,” *Ther. Adv. Neurol. Disord.*, vol. 2, no. 6, pp. 20–28, Nov. 2009, doi: 10.1177/1756285609339382.

[73] R. Ramasubbu, S. Lang, and Z. H. T. Kiss, “Dosing of Electrical Parameters in Deep Brain Stimulation (DBS) for Intractable Depression: A Review of Clinical Studies,” *Front. Psychiatry*, vol. 9, 2018, Accessed: Dec. 05, 2022. [Online]. Available: https://www.frontiersin.org/articles/10.3389/fpsyt.2018.00302

[74] “Intan Technologies,” *Intan Technologies*. https://www.intantech.com (accessed Dec. 05, 2022).

[75] W. Jung, Ed., “SECTION 5-4 - Standard Responses,” in *Op Amp Applications Handbook*, Burlington: Newnes, 2005, pp. 325–348. doi: 10.1016/B978-075067844-5/50137-5.

[76] H. Bokil, P. Andrews, J. E. Kulkarni, S. Mehta, and P. Mitra, “Chronux: A Platform for Analyzing Neural Signals,” *J. Neurosci. Methods*, vol. 192, no. 1, pp. 146–151, Sep. 2010, doi: 10.1016/j.jneumeth.2010.06.020.

[77] B. Babadi and E. N. Brown, “A Review of Multitaper Spectral Analysis,” *IEEE Trans. Biomed. Eng.*, vol. 61, no. 5, pp. 1555–1564, May 2014, doi: 10.1109/TBME.2014.2311996.

[78] M. J. Prerau, R. E. Brown, M. T. Bianchi, J. M. Ellenbogen, and P. L. Purdon, “Sleep Neurophysiological Dynamics Through the Lens of Multitaper Spectral Analysis,” *Physiology*, vol. 32, no. 1, pp. 60–92, Jan. 2017, doi: 10.1152/physiol.00062.2015.

[79] D. P. Nguyen, M. A. Wilson, E. N. Brown, and R. Barbieri, “Measuring Instantaneous Frequency of Local Field Potential Oscillations using the Kalman Smoother,” *J. Neurosci. Methods*, vol. 184, no. 2, pp. 365–374, Nov. 2009, doi: 10.1016/j.jneumeth.2009.08.012.

[80] “JoVE | Peer Reviewed Scientific Video Journal - Methods and Protocols.” https://www.jove.com/pdf/53066 (accessed Dec. 05, 2022).

[81] A. Andree *et al.*, “Deep brain stimulation electrode modeling in rats,” *Exp. Neurol.*, vol. 350, p. 113978, Apr. 2022, doi: 10.1016/j.expneurol.2022.113978.

[82] L.-M. Schönfeld and L. Wojtecki, “Beyond Emotions: Oscillations of the Amygdala and Their Implications for Electrical Neuromodulation,” *Front. Neurosci.*, vol. 13, 2019, Accessed: Dec. 05, 2022. [Online]. Available: https://www.frontiersin.org/articles/10.3389/fnins.2019.00366

[83] E. M. Prager, H. C. Bergstrom, G. H. Wynn, and M. F. M. Braga, “The Basolateral Amygdala GABAergic System in Health and Disease,” *J. Neurosci. Res.*, vol. 94, no. 6, pp. 548–567, Jun. 2016, doi: 10.1002/jnr.23690.

[84]A. R. Woodruff, H. Monyer, and P. Sah, “GABAergic excitation in the basolateral amygdala,” *J. Neurosci. Off. J. Soc. Neurosci.*, vol. 26, no. 46, pp. 11881–11887, Nov. 2006, doi: 10.1523/JNEUROSCI.3389-06.2006.

[85] R. Nakajima *et al.*, “Comprehensive behavioral analysis of heterozygous Syngap1 knockout mice,” *Neuropsychopharmacol. Rep.*, vol. 39, no. 3, pp. 223–237, Sep. 2019, doi: 10.1002/npr2.12073.

[86] M. Leger *et al.*, “Object recognition test in mice,” *Nat. Protoc.*, vol. 8, no. 12, Art. no. 12, Dec. 2013, doi: 10.1038/nprot.2013.155.

[87] S. S. Moy *et al.*, “Sociability and preference for social novelty in five inbred strains: an approach to assess autistic-like behavior in mice,” *Genes Brain Behav.*, vol. 3, no. 5, pp. 287–302, Oct. 2004, doi: 10.1111/j.1601-1848.2004.00076.x.

[88] M. Kilinc *et al.*, “Endogenous Syngap1 alpha splice forms promote cognitive function and seizure protection,” *eLife*, vol. 11, p. e75707, Apr. 2022, doi: 10.7554/eLife.75707.

[89] J. P. Clement *et al.*, “Pathogenic SYNGAP1 Mutations Impair Cognitive Development by Disrupting Maturation of Dendritic Spine Synapses,” *Cell*, vol. 151, no. 4, pp. 709–723, Nov. 2012, doi: 10.1016/j.cell.2012.08.045.

[90] M. Z. Awad *et al.*, “Subcortical short-term plasticity elicited by deep brain stimulation,” *Ann. Clin. Transl. Neurol.*, vol. 8, no. 5, pp. 1010–1023, Apr. 2021, doi: 10.1002/acn3.51275.

[91] A. M. Saleh, T. VanDyk, K. R. Jacobson, S. Calve, and T. L. Kinzer-Ursem, “An Integrative Biology Approach to Quantify the Biodistribution of Azidohomoalanine In Vivo,” Jun. 2021. doi: 10.1101/2021.06.14.448308.

[92] S. tom Dieck *et al.*, “Direct visualization of newly synthesized target proteins in situ,” *Nat. Methods*, vol. 12, no. 5, Art. no. 5, May 2015, doi: 10.1038/nmeth.3319.